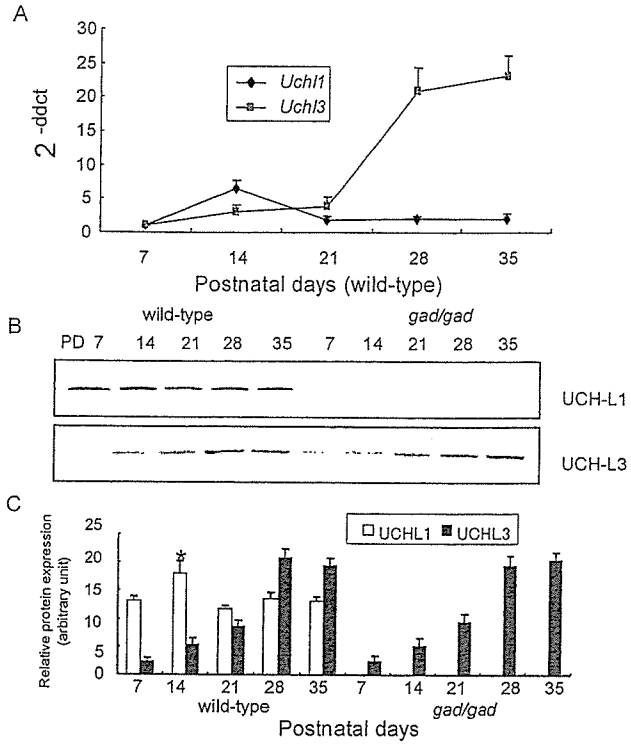

FIG. 1. Expression of UCHL1 and UCHL3during the first round of spermatogenesis. A) Comparison of *Uchl1* and *Uchl3* gene expression levels (2^{-ddCt}) by SYBR Green-based real-time quantitative reverse transcription-polymerase chain reaction (RT-PCR). The value for gene expression from the testes of 7-day-old mice was set to 1.0. B) Comparison of UCHL1 and UCHL3 expression by Western blotting of testicular lysates from wild-type or *gad* mice. Blots were reprobed for α-tubulin, which was used to normalize the protein load. Representative images from four independent experiments are shown. C) Quantitative analysis of changes in UCHL1 and UCHL3 levels by Western blotting. Relative protein expression (optical density) of the bands in panel B, normalized to α-tubulin. Each data point represents the mean ± SD (n = 4; * $P < 0.05$).

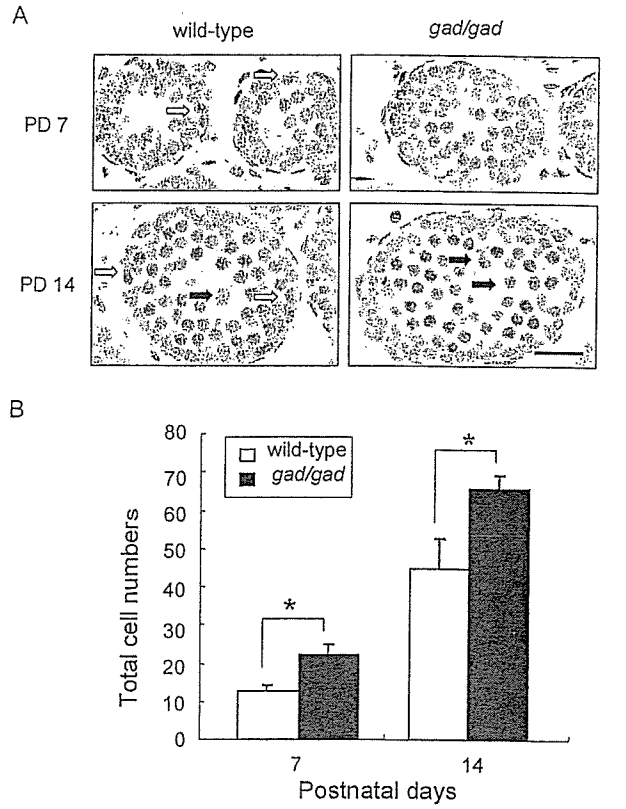

FIG. 2. A) Immunohistochemistry of UCHL1 and testicular morphology during the first round of spermatogenesis. UCHL1-positive germ cells in wild-type mice are indicated by open arrows. Spermatogonia and preleptotene spermatocytes (closed arrows) were more abundant and found further from the basement membrane in Postnatal Day (PD) 7 and 14 *gad* mice. Magnification ×200. Bar = 20 μm. B) The total number of germ cells in seminiferous tubules was significantly increased in and 7- and 14-day-old *gad* mice compared with wild-type mice (n = 4; * $P < 0.05$). Data represent mean ± SD.

based real-time quantitative RT-PCR (Fig. 1A). Despite the fact that the percentage of spermatogonia and Sertoli cells may be diluted by meiotic and postmeiotic germ cells after Day 14 [20], *Uchl1* expression was high in 14-day-old mice, in agreement with our previous findings.

Immunohistochemistry of UCHL1 and Quantitative Morphometric Assessment

Immunohistochemical analysis revealed UCHL1 expression in spermatogonia from wild-type mice but not *gad* mice (Fig. 2A). Preliminary examination of tubules from immature testes revealed an overproduction of germ cells in *gad* mice. At 7 and 14 days of age, the number of spermatogonia and preleptotene spermatocytes was significantly increased in *gad* mice compared with wild-type mice (Fig. 2A). The increase in the number of these cell types was further confirmed by quantitative analysis, which showed that the total number of testicular cells, including Sertoli cells, was significantly higher in 7- and 14-day-old *gad* mice (Fig. 2B).

TUNEL Staining of Apoptotic Germ Cells During the First Round of Spermatogenesis

To further investigate the mechanism underlying the observed differences in testicular cell numbers between wild-type and *gad* mice during the first round of spermatogenesis, we examined germ cell apoptosis in tissue sections from mice at 7, 14, 21, 28, and 35 days of age by TUNEL assay. During the first round of spermatogenesis, the total number of apoptotic cells in 20 circular seminiferous tubules decreased significantly (n = 4; $P < 0.05$) in gad mouse testes as compared with wild-type mice (Fig. 3A). Although germ cell apoptosis significantly increased at Day 14 in the testes of both wild-type and *gad* mice, *gad* mice had significantly fewer apoptotic germ cells (n = 4; $P <$ 0.05) in seminiferous tubules (Fig. 3B).

Testicular Germ Cells of gad *Mice Are Resistant to Apoptosis-Inducing Conditions In Vitro*

Sertoli cells, which support germ cells, express UCHL1 [12]. To explore the viability of germ cells independently of the effect of Sertoli cells, testicular germ cells from 2-wk-old wild-type and *gad* mice were cultured in suspension for 5 days in the presence of 10% FBS. We then examined the resistance of these in vitro cell culture to apoptosis-inducing conditions. Although both wild-type and *gad* mouse cells were sensitive to apoptosis-inducing conditions, the *gad* mouse cells had comparatively greater viability (Fig. 4). Overall results clearly show that the absence of UCHL1 increase germ cell survival.

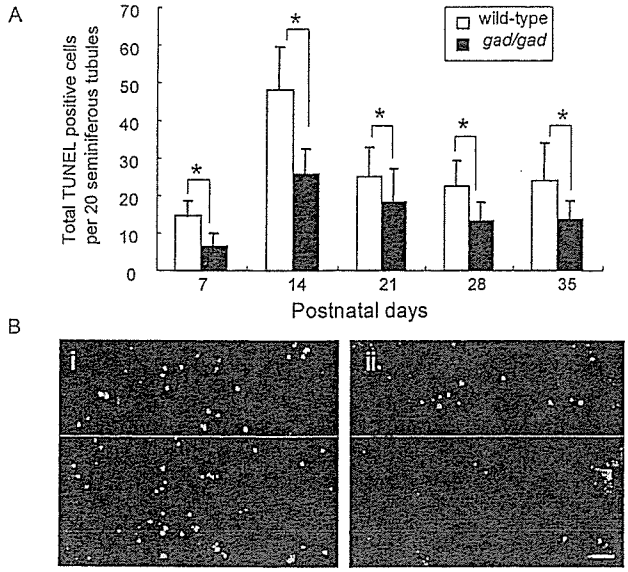

FIG. 3. A) The total TUNEL-positive germinal cells per 20 circular seminiferous tubules in wild-type and *gad* mice on various postnatal days. In each group, the data represent the mean ± SD (n = 4; * $P < 0.05$). B) The extent of apoptosis in 2-wk-old mice. i, wild-type mice; ii, *gad* mice. Green fluorescence, TUNEL-positive cells; red fluorescence, nuclei stained with propidium iodide. Magnification ×100. Bar = 30 μm.

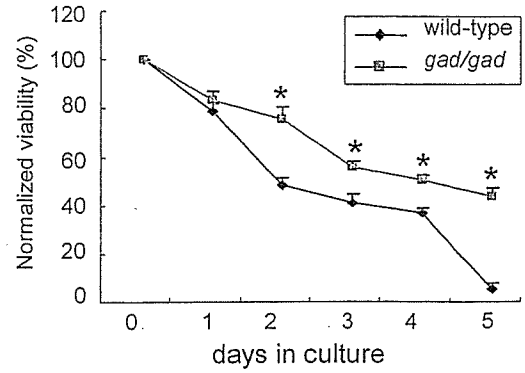

FIG. 4. In vitro survival of testicular germ cells. Testicular germ cells were isolated from wild-type and *gad* mice at 14 days of age. After culture, viability was determined using a Vi-Cell XR cell viability analyzer (Beckman Coulter). Viability at each time point was normalized to that at Day 0. Each data point represents the mean ± SD (n = 4; * $P < 0.05$).

Levels of Apoptotic Proteins During the First Round of Spermatogenesis

Germ cell apoptosis involves genes encoding various factors, such as *Trp53*, the *Bcl2* family, and *caspase*, which are targets for ubiquitination [29–31]. Our previous work demonstrated that the expression of antiapoptotic proteins (Bcl2 family and XIAP) is significantly elevated following cryptorchid stress in *gad* mice [22]. To explore whether the germ cell apoptotic wave is associated with changes in the levels of proteins known to be associated with cell death or survival, Western blot analysis was performed on testicular lysates obtained from 7-, 14-, 21-, 28-, and 35-day-old wild-type and *gad* mice (Fig. 5). Levels of TRP53 and Bax proteins were strikingly elevated in 7-day-old mice but barely detectable on Day 35. Caspase-3 was also strikingly elevated in 7-day-old mice. Since TRP53 modulates Bax expression [22, 32], the observed up-regulation of Bax is consistent with elevated TRP53 levels during the early apoptotic wave. Expression of the antiapoptotic protein Bcl-xL was weaker in immature compared with mature testes. Levels of TRP53, Bax, and caspase-3 proteins were significantly decreased in 7- and 14-day-old *gad* mice relative to the levels observed in wild-type testes (Fig. 5B). By contrast, the level of Bcl-xL protein appeared to be up-regulated earlier in *gad* mice (at 28 days) than in wild-type mice (at 35 days) (Fig. 5B).

Assessment of Cauda Epididymidis and Spermatozoa Morphology in gad *Mice*

The cauda epididymidis from wild-type and *gad* mice were weighed, and the sperm were collected and analyzed. The cauda epididymidis from *gad* mice weighed significantly less, likely resulting from the lower sperm concentration measured in *gad* mice (19.5 × 10^6/ml) compared with wild-type mice (23.6 × 10^6/ml) (Table 1). Furthermore, abnormal sperm morphology, including head and midpiece defects or a detached head, occurred significantly more often in *gad* mice (Table 1 and Fig. 6A). Immunocytochemical analysis showed that UCHL1 and ubiquitin were expressed in defective spermatozoa but not in normal spermatozoa (Fig. 6B). Ubiquitin, a marker for sperm abnormalities [33], was detected mainly in defective spermatozoa. However, despite a significantly elevated number of defective spermatozoa, ubiquitin expression in *gad* mouse spermatozoa was similar to that in wild-type mice (data not shown).

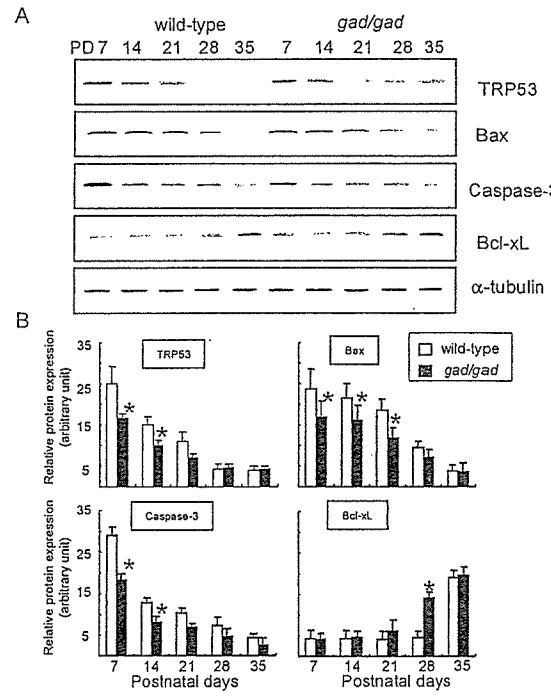

FIG. 5. A) Western blot analyses showing TRP53, Bax, caspase-3, and Bcl-xL levels in wild-type and *gad* mice during the first round of spermatogenesis. Protein (5 μg/lane) was prepared from whole testes at 7, 14, 21, 28, and 35 days of age. Blots were reprobed for α-tubulin to normalize for differences in the amount of protein loaded. Representative images of four independent experiments are shown. B) Quantitative Western blot analysis of changes in TRP53, Bax, caspase-3, and Bcl-xL levels. Relative protein expression (optical density) of the bands in panel A, normalized to α-tubulin. Each data point represents the mean ± SD (n = 4; * $P < 0.05$).

TABLE 1. Analysis of epididymal tail weight and sperm morphology (mean ± SD) in 10-week-old wild-type and *gad* mice.

	Tail weight (mg)	Sperm concentration (10^6/ml)	Defect (%)			
			Head	Midpiece	Principal piece	Detached head
wild-type	30.0 ± 0.8	23.6 ± 3.7	7.2 ± 1.5	2.4 ± 1.3	1.1 ± 0.2	2.0 ± 1.0
gad/gad	24.7 ± 1.1*	19.5 ± 3.3*	14.1 ± 2.8*	4.7 ± 1.5*	1.7 ± 0.6	3.7 ± 1.2*

* Significantly different from wild-type mice (n = 7; $P < 0.05$).

Spermatozoa Motility in gad *Mice*

We measured sperm motility parameters in wild-type and *gad* mice. Of the parameters assessed, MSP, PMP, VAP (μm/sec), VSL (μm/sec), and VCL (μm/sec) were significantly lower in *gad* mice. ALH (μm), linearity (%), and straightness (%) did not differ significantly between *gad* and wild-type mice (Fig. 7). Of the parameters we measured, the number of PMP differed most significantly between *gad* mice (24.4%) and wild-type mice (34.3%) (Fig. 7A).

DISCUSSION

Spermatogenesis is a highly complex process involving male germ cell proliferation and maturation from spermatogonia to spermatozoa [34]. Apoptosis is common during this process and is believed to play an important role in controlling germ cell numbers and eliminating defective germ cells that carry DNA mutations, thus ensuring the production of intact, functional spermatozoa [35–37]. Normally, germ cells are extremely sensitive to DNA damage, as such lesions are incompatible with the ultimate function of these cells [23, 24, 37]. The early apoptotic wave may result in early elimination of defective germ cells in which DNA alterations have occurred through chromosomal crossing over during the first meiotic division [23, 24, 37].

Several lines of evidence indicate that UCHL1 associates with monoubiquitin and that the monoubiquitin pool is reduced in *gad* mice relative to wild-type mice [18, 19, 22]. Furthermore, testes from UCHL1-deficient *gad* mice [22] and mice carrying the K48R mutation in ubiquitin [38] show resistance to cryptorchid-induced apoptosis, suggesting that ubiquitin is critical for modulating testicular germ cell death. Normally, damaged proteins are polyubiquitinated and degraded via the ubiquitin-proteasome system; however, if damaged proteins are not degraded as easily when monoubiquitin is either mutated or reduced [22, 38], then germinal cells may become resistant to programmed death. Our results with the *gad* mouse suggest that ubiquitin induction is important for regulating programmed germinal cell death that is normally observed during the first round of spermatogenesis. We have now shown that immature testes from *gad* mice are resistant to the massive wave of germinal cell apoptosis during the first round of spermatogenesis. The increased resistance of UCHL1-deficient germ cells to apoptosis-inducing conditions in vivo and in vitro suggests that UCHL1 is involved in spermatogenesis (Figs. 3 and 4). The activity of the ubiquitin-proteasome system may be required for specific transitions between multiple developmental cellular processes and sequential apoptosis during spermatogenesis [6, 7, 39]. In addition, the ubiquitin-proteasome system is required for the degradation or modification of numerous germ cell-specific proteins during different phases of spermatogenesis [39–41].

Early apoptosis in testicular germ cells is regulated by a complicated signal transduction pathway. The testes contain high levels of TRP53, Bcl2 family, and caspase-3 proteins, which are targets for ubiquitination [29–31, 42–45]. However, the involvement of the ubiquitin system in the regu-

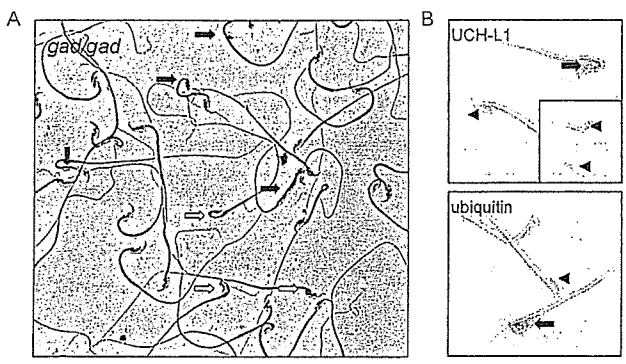

FIG. 6. A) Abnormal morphology of spermatozoa from *gad* mice. Spermatozoa were collected from the cauda epididymidis of 10-wk-old *gad* mice. Head defects (open arrows) and midpiece defects (closed arrows) are indicated. Magnification ×400. B) Immunocytochemistry of UCH-L1 and ubiquitin in wild-type and *gad* mice. UCHL1- and ubiquitin-positive spermatozoa (closed arrows) and normal spermatozoa (both negative, arrowheads) in wild-type mice are indicated. The inset shows an the image of spermatozoa from *gad* mice. Magnification ×1000.

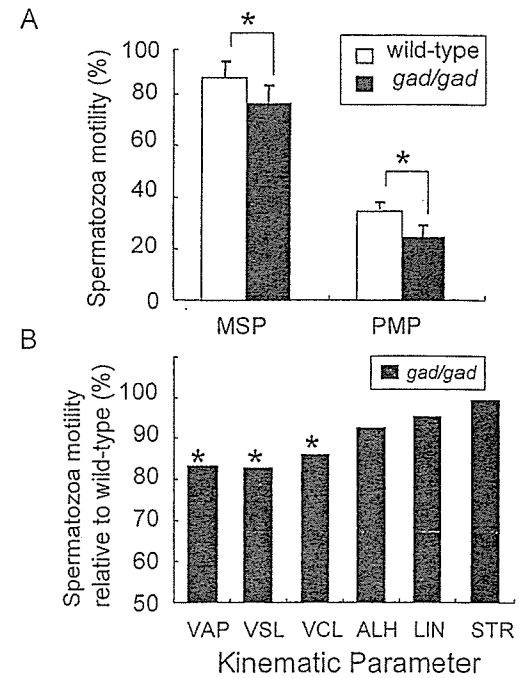

FIG. 7. Kinematic analysis of spermatozoa from the cauda epididymidis of 10-week-old wild-type and *gad* mice. A) Sperm motility. MSP, Percentage of motile sperm; PMP, Percentage of progressively motile sperm (n = 7; * $P < 0.05$). Data represent the mean ± SD. B) Movement characterization. VAP, Average path velocity (μm/sec); VSL, Straight-line velocity (μm/sec); VCL, Curvilinear velocity (μm/sec); ALH, Lateral head displacement (μm); LIN, Linearity (VSL/VCL × 100); STR, Straightness (VSL/VAP × 100). Data are expressed as a percentage of the values obtained for each parameter in wild-type mice (n = 7; * $P < 0.05$).

latory mechanisms of germ cell apoptosis has not been identified. A previous study showed that UCHL1-deficient *gad* mice express high levels of antiapoptotic proteins (Bcl2 family and XIAP) in the testis following cryptorchid-induced stress [22]. Alterations in the carefully maintained balance between the expression of apoptosis-inducing and apoptosis-protecting proteins may constitute one mechanism underlying the suppression of germ cell apoptosis observed in *gad* mice [46]. The decreased levels of TRP53, Bax, and caspase-3 observed in *gad* mice in this study are consistent with the suppression of germ cell apoptosis. In addition, the expression of the antiapoptotic protein Bcl-xL increased earlier in *gad* mice compared with wild-type mice. Therefore, the control of the apoptotic wave probably depends on variations in the balance between Bax and Bcl-xL [23, 47]. Analysis of the first round of spermatogenesis over time demonstrated a striking and massive wave of apoptotic germinal cells in 14-day-old mice (Fig. 3). High levels of UCHL1 protein were also observed at this age (Fig. 1) [20]. This early apoptotic wave was suppressed in the testes of *gad* mice, which had an abundance of germ cells compared with wild-type mice (Fig. 2). Moreover, the suppression of germ cell death is consistent with our previous report on cryptorchid stress injury in *gad* mice [22]. The testes of *gad* mice showed a phenotype similar to that of *Bax*-deficient mice or those overexpressing *Bcl2* or *Bcl-xL* [23, 25, 26]. Also, the testes of *Trp53*$^{-/-}$ mice exhibited a similar phenotype involving decreased germ cell apoptosis and an increased number of germ cells [48].

In the present study, we also characterized spermatozoa in *gad* mice with regard to the following reproductive endpoints: 1) the weight of reproductive organs, 2) the concentration of sperm cells, and 3) the motility and morphology of spermatozoa collected from the cauda epididymidis. The weight of cauda epididymidis from *gad* mice was significantly lower compared with that from wild-type mice. The concentration of sperm cells was also significantly lower, and most motility parameters of spermatozoa collected from the cauda epididymidis were affected in *gad* mice (Fig. 7). The significant decline in progressive forward motility, VAP, VSL, and VCL indicates that UCHL1 deficiency affects not only the ability of spermatozoa to move in the forward direction but also their vigor. In addition, the percentage of morphologically abnormal spermatozoa was significantly higher in *gad* mice (Table 1 and Fig. 6A).

Sperm production in the testis is a regulated balance between germ cell division and germ cell loss [26, 49], and there is emerging evidence that the ubiquitin-proteasome system may be central to the coordination of this process. For example, during spermatogenesis, the general activity of the ubiquitin-proteasome system is high, probably reflecting the requirement for massive degradation of cytoplasmic and nuclear proteins [6, 7, 50, 51]. Additionally, mutation of the ubiquitin-conjugating enzyme HR6B results in impaired spermatogenesis during nuclear condensation in spermatids [39, 41]. We found the fact that UCH-L1 associates with monoubiquitin in several lines of *gad* mice [18, 19, 22]. Furthermore, both proteins are expressed abundantly and at comparable levels in testis and the epididymis [11, 13, 14], suggesting that the functions of two proteins are important during spermatogenesis. Ubiquitin is present in defective spermatozoa, and proteins in these cells become ubiquitinated during epididymal passage (Fig. 6B) [11, 14, 33, 52, 53]. Furthermore, ubiquitination in the epididymis may trigger apoptotic mechanisms that recognize and eliminate abnormal spermatozoa [49, 54, 55].

Further study is required to elucidate the functional significance of the association between UCHL1 and ubiquitin during spermatozoa maturation in the epididymis. However, our observations suggest that UCHL1 may function to regulate sperm production and to ubiquitinate proteins in defective spermatozoa. Our present study demonstrates that UCHL1-deficient *gad* mice are resistant to the wave of germinal cell apoptosis that occurs during the first round of spermatogenesis and that these mice have defects in sperm production, motility, and morphology. These results suggest that UCHL1 functions in the early apoptotic wave during the first round of spermatogenesis and in the control of sperm quality during sperm maturation.

ACKNOWLEDGMENTS

We thank H. Kikuchi for technical assistance with tissue sections and M. Shikama for the care and breeding of animals.

REFERENCES

1. Ciechanover A, Finley D, Varshavsky A. Ubiquitin dependence of selective protein degradation demonstrated in the mammalian cell cycle mutant ts85. Cell 1984; 37:57–66.
2. Glotzer M, Murray AW, Kirschner MW. Cyclin is degraded by the ubiquitin pathway. Nature 1991; 349:132–138.
3. Strous GJ, Govers R. The ubiquitin-proteasome system and endocytosis. J Cell Sci 1999; 112(pt 10):1417–1423.
4. Wilkinson KD. Regulation of ubiquitin-dependent processes by deubiquitinating enzymes. FASEB J 1997; 11:1245–1256.
5. Hershko A, Ciechanover A. The ubiquitin system. Annu Rev Biochem 1998; 67:425–479.
6. Baarends WM, Roest HP, Grootegoed JA. The ubiquitin system in gametogenesis. Mol Cell Endocrinol 1999; 151:5–16.
7. Baarends WM, van der Laan R, Grootegoed JA. Specific aspects of the ubiquitin system in spermatogenesis. J Endocrinol Invest 2000; 23:597–604.
8. Ciechanover A. The ubiquitin-proteasome pathway: on protein death and cell life. EMBO J 1998; 17:7151–7160.
9. Weissman AM. Themes and variations on ubiquitylation. Nat Rev Mol Cell Biol 2001; 2:169–178.
10. Wing SS. Deubiquitinating enzymes—the importance of driving in reverse along the ubiquitin-proteasome pathway. Int J Biochem Cell Biol 2003; 35:590–605.
11. Fraile B, Martin R, De Miguel MP, Arenas MI, Bethencourt FR, Peinado F, Paniagua R, Santamaria L. Light and electron microscopic immunohistochemical localization of protein gene product 9.5 and ubiquitin immunoreactivities in the human epididymis and vas deferens. Biol Reprod 1996; 55:291–297.
12. Kon Y, Endoh D, Iwanaga T. Expression of protein gene product 9.5, a neuronal ubiquitin C-terminal hydrolase, and its developing change in sertoli cells of mouse testis. Mol Reprod Dev 1999; 54:333–341.
13. Kwon J, Kikuchi T, Setsuie R, Ishii Y, Kyuwa S, Yoshikawa Y. Characterization of the testis in congenitally ubiquitin carboxy-terminal hydrolase-1 (Uch-L1) defective (gad) mice. Exp Anim 2003; 52:1–9.
14. Martin R, Santamaria L, Fraile B, Paniagua R, Polak JM. Ultrastructural localization of PGP 9.5 and ubiquitin immunoreactivities in rat ductus epididymidis epithelium. Histochem J 1995; 27:431–439.
15. Pickart CM, Rose IA. Ubiquitin carboxyl-terminal hydrolase acts on ubiquitin carboxyl-terminal amides. J Biol Chem 1985; 260:7903–7910.
16. Liu Y, Fallon L, Lashuel HA, Liu Z, Lansbury PT, Jr. The UCH-L1 gene encodes two opposing enzymatic activities that affect alpha-synuclein degradation and Parkinson's disease susceptibility. Cell 2002; 111:209–218.
17. Liu Y, Lashuel HA, Choi S, Xing X, Case A, Ni J, Yeh LA, Cuny GD, Stein RL, Lansbury PT, Jr. Discovery of inhibitors that elucidate the role of UCH-L1 activity in the H1299 lung cancer cell line. Chem Biol 2003; 10:837–846.
18. Osaka H, Wang YL, Takada K, Takizawa S, Setsuie R, Li H, Sato Y, Nishikawa K, Sun YJ, Sakurai M, Harada T, Hara Y, Kimura I, Chiba S, Namikawa K, Kiyama H, Noda M, Aoki S, Wada K. Ubiquitin carboxy-terminal hydrolase L1 binds to and stabilizes monoubiquitin in neuron. Hum Mol Genet 2003; 12:1945–1958.

19. Harada T, Harada C, Wang YL, Osaka H, Amanai K, Tanaka K, Takizawa S, Setsuie R, Sakurai M, Sato Y, Noda M, Wada K. Role of ubiquitin carboxy terminal hydrolase-L1 in neural cell apoptosis induced by ischemic retinal injury in vivo. Am J Pathol 2004; 164:59–64.
20. Kwon J, Wang YL, Setsuie R, Sekiguchi S, Sakurai M, Sato Y, Lee WW, Ishii Y, Kyuwa S, Noda M, Wada K, Yoshikawa Y. Developmental regulation of ubiquitin C-terminal hydrolase isozyme expression during spermatogenesis in mice. Biol Reprod 2004; 71:515–521.
21. Saigoh K, Wang YL, Suh JG, Yamanishi T, Sakai Y, Kiyosawa H, Harada T, Ichihara N, Wakana S, Kikuchi T, Wada K. Intragenic deletion in the gene encoding ubiquitin carboxy-terminal hydrolase in gad mice. Nat Genet 1999; 23:47–51.
22. Kwon J, Wang YL, Setsuie R, Sekiguchi S, Sato Y, Sakurai M, Noda M, Aoki S, Yoshikawa Y, Wada K. Two closely related ubiquitin C-terminal hydrolase isozymes function as reciprocal modulators of germ cell apoptosis in cryptorchid testis. Am J Pathol 2004; 165: 1367–1374.
23. Rodriguez I, Ody C, Araki K, Garcia I, Vassalli P. An early and massive wave of germinal cell apoptosis is required for the development of functional spermatogenesis. EMBO J 1997; 16:2262–2270.
24. Jahnukainen K, Chrysis D, Hou M, Parvinen M, Eksborg S, Soder O. Increased apoptosis occurring during the first wave of spermatogenesis is stage-specific and primarily affects midpachytene spermatocytes in the rat testis. Biol Reprod 2004; 70:290–296.
25. Furuchi T, Masuko K, Nishimune Y, Obinata M, Matsui Y. Inhibition of testicular germ cell apoptosis and differentiation in mice misexpressing Bcl-2 in spermatogonia. Development 1996; 122:1703–1709.
26. Russell LD, Chiarini-Garcia H, Korsmeyer SJ, Knudson CM. Bax-dependent spermatogonia apoptosis is required for testicular development and spermatogenesis. Biol Reprod 2002; 66:950–958.
27. Slott VL, Suarez JD, Perreault SD. Rat sperm motility analysis: methodologic considerations. Reprod Toxicol 1991; 5:449–458.
28. Goyal HO, Braden TD, Mansour M, Williams CS, Kamaleldin A, Srivastava KK. Diethylstilbestrol-treated adult rats with altered epididymal sperm numbers and sperm motility parameters, but without alterations in sperm production and sperm morphology. Biol Reprod 2001; 64:927–934.
29. Chipuk JE, Green DR. Cytoplasmic p53: Bax and forward. Cell Cycle 2004; 3:429–431.
30. Dimmeler S, Breitschopf K, Haendeler J, Zeiher AM. Dephosphorylation targets Bcl-2 for ubiquitin-dependent degradation: a link between the apoptosome and the proteasome pathway. J Exp Med 1999; 189:1815–1822.
31. Suzuki Y, Nakabayashi Y, Takahashi R. Ubiquitin-protein ligase activity of X-linked inhibitor of apoptosis protein promotes proteasomal degradation of caspase-3 and enhances its anti-apoptotic effect in Fas-induced cell death. Proc Natl Acad Sci U S A 2001; 98:8662–8667.
32. Selvakumaran M, Lin HK, Miyashita T, Wang HG, Krajewski S, Reed JC, Hoffman B, Liebermann D. Immediate early upregulation of bax expression by p53 but not TGF beta 1: a paradigm for distinct apoptotic pathways. Oncogene 1994; 9:1791–1798.
33. Sutovsky P, Moreno R, Ramalho-Santos J, Dominko T, Thompson WE, Schatten G. A putative, ubiquitin-dependent mechanism for the recognition and elimination of defective spermatozoa in the mammalian epididymis. J Cell Sci 2001; 114:1665–1675.
34. de Kretser DM, Loveland KL, Meinhardt A, Simorangkir D, Wreford N. Spermatogenesis. Hum Reprod 1998; 13(suppl 1):1–8.
35. Gosden R, Spears N. Programmed cell death in the reproductive system. Br Med Bull 1997; 53:644–661.
36. Matsui Y. Regulation of germ cell death in mammalian gonads. APMIS 1998; 106:142–147Ascussion 147–148.
37. Print CG, Loveland KL. Germ cell suicide: new insights into apoptosis during spermatogenesis. Bioessays 2000; 22:423–430.
38. Rasoulpour RJ, Schoenfeld HA, Gray DA, Boekelheide K. Expression of a K48R mutant ubiquitin protects mouse testis from cryptorchid injury and aging. Am J Pathol 2003; 163:2595–2603.
39. Baarends WM, Wassenaar E, Hoogerbrugge JW, van Cappellen G, Roest HP, Vreeburg J, Ooms M, Hoeijmakers JH, Grootegoed JA. Loss of HR6B ubiquitin-conjugating activity results in damaged synaptonemal complex structure and increased crossing-over frequency during the male meiotic prophase. Mol Cell Biol 2003; 23:1151–1162.
40. Baarends WM, Hoogerbrugge JW, Roest HP, Ooms M, Vreeburg J, Hoeijmakers JH, Grootegoed JA. Histone ubiquitination and chromatin remodeling in mouse spermatogenesis. Dev Biol 1999; 207: 322–333.
41. Roest HP, van Klaveren J, de Wit J, van Gurp CG, Koken MH, Vermey M, van Roijen JH, Hoogerbrugge JW, Vreeburg JT, Baarends WM, Bootsma D, Grootegoed JA, Hoeijmakers JH. Inactivation of the HR6B ubiquitin-conjugating DNA repair enzyme in mice causes male sterility associated with chromatin modification. Cell 1996; 86: 799–810.
42. Marshansky V, Wang X, Bertrand R, Luo H, Duguid W, Chinnadurai G, Kanaan N, Vu MD, Wu J. Proteasomes modulate balance among proapoptotic and antiapoptotic Bcl-2 family members and compromise functioning of the electron transport chain in leukemic cells. J Immunol 2001; 166:3130–3142.
43. Oren M. Regulation of the p53 tumor suppressor protein. J Biol Chem 1999; 274:36031–36034.
44. Orlowski RZ. The role of the ubiquitin-proteasome pathway in apoptosis. Cell Death Differ 1999; 6:303–313.
45. Yang Y, Yu X. Regulation of apoptosis: the ubiquitous way. FASEB J 2003; 17:790–799.
46. Beumer TL, Roepers-Gajadien HL, Gademan IS, Lock TM, Kal HB, De Rooij DG. Apoptosis regulation in the testis: involvement of Bcl-2 family members. Mol Reprod Dev 2000; 56:353–359.
47. Borner C. The Bcl-2 protein family: sensors and checkpoints for life-or-death decisions. Mol Immunol 2003; 39:615–647.
48. Yin Y, Stahl BC, DeWolf WC. Morgentaler A. p53-mediated germ cell quality control in spermatogenesis. Dev Biol 1998; 204:165–171.
49. Sutovsky P. Ubiquitin-dependent proteolysis in mammalian spermatogenesis, fertilization, and sperm quality control: killing three birds with one stone. Microsc Res Tech 2003; 61:88–102.
50. Rajapurohitam V, Bedard N, Wing SS. Control of ubiquitination of proteins in rat tissues by ubiquitin conjugating enzymes and isopeptidases. Am J Physiol Endocrinol Metab 2002; 282:E739–E745.
51. Rajapurohitam V, Morales CR, El-Alfy M, Lefrancois S, Bedard N, Wing SS. Activation of a UBC4-dependent pathway of ubiquitin conjugation during postnatal development of the rat testis. Dev Biol 1999; 212:217–228.
52. Lippert TH, Seeger H, Schieferstein G, Voelter W. Immunoreactive ubiquitin in human seminal plasma. J Androl 1993; 14:130–131.
53. Sutovsky P, Terada Y, Schatten G. Ubiquitin-based sperm assay for the diagnosis of male factor infertility. Hum Reprod 2001; 16:250–258.
54. Sinha Hikim AP, Swerdloff RS. Hormonal and genetic control of germ cell apoptosis in the testis. Rev Reprod 1999; 4:38–47.
55. Sutovsky P, Hauser R, Sutovsky M. Increased levels of sperm ubiquitin correlate with semen quality in men from an andrology laboratory clinic population. Hum Reprod 2004; 19:628–638.

Journal of Neurochemistry, 2005, **92**, 1061–1072 doi:10.1111/j.1471-4159.2004.02963.x

Potentiation of ATP-induced currents due to the activation of P2X receptors by ubiquitin carboxy-terminal hydrolase L1

Yoshimasa Manago,* Yoshiko Kanahori,* Aki Shimada,* Ayumi Sato,* Taiju Amano,* Yae Sato-Sano,*,† Rieko Setsuie,*,† Mikako Sakurai,*,† Shunsuke Aoki,† Yu-Lai Wang,† Hitoshi Osaka,†,‡ Keiji Wada† and Mami Noda‡

**Laboratory of Pathophysiology, Graduate School of Pharmaceutical Sciences, Kyushu University, Fukuoka, Japan*

†Department of Degenerative Neurological Diseases, National Institute of Neuroscience, National Center of Neurology and Psychiatry, Tokyo, Japan

‡Information and Cellular function, PRESTO, Japan Science and Technology Corporation (JST), Kawaguchi, Saitama, Japan

Abstract

Mammalian neuronal cells abundantly express a de-ubiquitinating isozyme, ubiquitin carboxy-terminal hydrolase L1 (UCH L1). Loss of UCH L1 function causes dying-back type of axonal degeneration. However, the function of UCH L1 in neuronal cells remains elusive. Here we show that overexpression of UCH L1 potentiated ATP-induced currents due to the activation of P2X receptors that are widely distributed in the brain and involved in various biological activities including neurosecretion. ATP-induced inward currents were measured in mock-, wild-type or mutant (C90S)-UCH L1-transfected PC12 cells under the conventional whole-cell patch clamp configuration. The amplitude of ATP-induced currents was significantly greater in both wild-type and C90S UCH L1-transfected cells, suggesting that hydrolase activity was not involved but increased level of mono-ubiquitin might play an important role. The increased currents were dependent on cAMP-dependent protein kinase (PKA) and Ca^{2+} and calmodulin-dependent protein kinase (CaMKII) but not protein kinase C. In addition, ATP-induced currents were likely to be modified via dopamine and cyclic AMP-regulated phosphoprotein (DARPP-32) that is regulated by PKA and phosphatases. Our finding shows the first evidence that there is a relationship between UCH L1 and neurotransmitter receptor, suggesting that UCH L1 may play an important role in synaptic activity.

Keywords: CaMKII, DARPP-32, PKA, patch-clamp, PC12, UCH L1.

J. Neurochem. (2005) **92**, 1061–1072.

The ubiquitin-proteasome system is an evolutionarily conserved and energy-dependent proteolytic pathway that functions constitutively to degrade proteins. Recent studies indicate that ubiquitin-mediated proteolysis can also be regulated and is of widespread importance (Wilkinson 1995; Coux *et al.* 1996). Regulated proteolysis by the ubiquitin-

Received August 24, 2004; accepted October 8, 2004.

Address correspondence and reprint requests to Mami Noda, PhD, Laboratory of Pathophysiology, Graduate School of Pharmaceutical Sciences Kyushu University, 3-1-1 Maidashi, Higashi-ku, Fukuoka 812–8582, Japan, Tel./Fax: + 81-92-642-6574.
E-mail: noda@phar.kyushu-u.ac.jp

Abbreviations used: ATP, adenosine triphosphate; BSA, bovine serum albumin; CaMKII, Ca^{2+} and calmodulin-dependent protein kinase; CDK, cyclin-dependent kinase; CHO, cells, Chinese hamster ovary cells; CREB, Ca^{2+}-stimulated cAMP response element binding protein; DAPI, 4′, 6-diamidino-2-phenylindole, dihydrochloride; EGTA, ethyleneglycol-bis-N, N, N′, N′-tetraacetic acid; ERK, extracellular signal-regulated kinase; DARPP-32, dopamine and cyclic AMP-regulated phosphoprotein with molecular weight of about 32 000; 1,9-dideoxyforskolin, 7β-acetoxy-6β-hydroxy-8,13-epoxy-labd-14-en-11-one; FBS, fetal bovine serum; forskolin, 7β-acetoxy-8,13-epoxy-1α,6β,9α-trihydroxy-labd-14-en-11-one; H-89, N-[2-(p-bromoocinamylamino)ethyl]-5-isoquinolinesulfonamide; HS, horse serum; KN-93, 2-[N-(2-hydroxyethyl)]-N-(4-methoxybenzenesulfonyl)]amino-N-(4-chlorocinnamyl)-N-methylbenzylamine); HEPES, N-2-hydroxyethylpiperazine-N′-2-ethansulfonic acid; MAPK, mitogen-activated protein kinase; NGF, nerve growth factor; PBS(–), Dulbecco's Ca^{2+}, Mg^{2+}-free phosphate buffer saline; PC12, cells, rat phenochromocytoma cells; PD98059, 2′-Amino-3′-methoxyflavone; PGP9.5, protein gene product 9.5; PKA, cyclic AMP-dependent protein kinase; PKC, protein kinase C; PP1, protein phosphatase 1; PP2, protein phosphatase 2; SDS-PAGE, sodium dodecyl sulfate-polyacrylamide gel electrophoresis; TBST, Tris buffer saline-Tween; Thr-34, threonine at 34; Thr-75, threonine at 75; Roscovitine, 2-(R)-(1-Ethyl-2-hydroxyethylamino)-6-benzylamino-9-isopropylpurine; UCH, L1, ubiquitin C-terminal hydrolase L1.

proteasome pathway has been implicated in the control of cell cycle (King *et al.* 1996), transcription activation (Verma *et al.* 1995), antigen presentation (Rock *et al.* 1994), cell fate and growth (Huang *et al.* 1995; Zhu *et al.* 1996), synaptogenesis (Muralidhar and Thomas 1993; Oh *et al.* 1994) and memory (Hegde *et al.* 1997). Ubiquitination of proteins is mediated by specific enzymes (E1, E2, and E3) and polyubiquitinated proteins are translocated to the 26S proteasome and subsequently proteolytically degraded (Ciechanover *et al.* 2000). Conversely, deubiquitination is thought to be essential for the regulation of proteolysis and for recycling of monoubiquitin from polyubiquitin chains.

Recently, one of the deubiquitinating enzymes, UCH L1 (ubiquitin carboxy-terminal hydrolase L1), was reported to be essential for brain function. UCH L1 is selectively expressed in neuron and testis (Wilkinson *et al.* 1989; Wilkinson *et al.* 1992). Loss of UCH L1 function was shown to cause neuronal degeneration observed in the gracile axonal dystrophy (*gad*) mouse (Saigoh *et al.* 1999), and missence mutation of UCH L1 was found in familial Parkinson disease (Leroy *et al.* 1998). As physiological functions of UCH L1, it is not limited to hydrolase activity; it has been shown that it associated with mono-ubiquitin and thus stabilized free ubiquitin by preventing its degradation within lysosomes. UCH L1's affinity for ubiquitin rather than hydrolase activity was required for the regulation of ubiquitin level (Osaka *et al.* 2003) and UCH L1 even might work as ubiquitin ligase (Liu *et al.* 2002). Furthermore, UCH L1 has been reported to have an important role in apoptosis in germ cell and neuron (Harada *et al.* 2004; Kwon *et al.* 2004b) and different UCH isozymes have distinct function during spermatogenesis (Kwon *et al.* 2004a).

As for neural function of UCH L1, little is known yet. In *Aplysia*, homologous UCH was shown to be important for learning and memory (Hegde *et al.* 1997). It is not yet known that UCH L1 works in a similar way in mammalian cells, but these results strongly suggest that UCH L1 plays an important role in synaptic function and morphology. In the present study, we investigated the neuronal function of UCH L1 on receptor channels which affect neurotransmitter secretion.

PC12 cells are often used as a model for studying neuronal cell function. Among neurotransmitter receptors expressed in PC12 cells, ATP receptors induce dopamine release (Sela *et al.* 1991). ATP receptors are divided into two subtypes, P2X and P2Y receptors. P2X receptors are ionotropic receptors and form cationic channels, while P2Y receptors are G-protein-coupled receptors and $P2Y_{1,\ 2,\ 4,\ 6,\ 11}$ cause intracellular Ca^{2+} mobilization via IP3 formation and activate Ca^{2+}-dependent K^+ channels (Ikeuchi *et al.* 1996). Among P2X receptors, $P2X_2$ and $P2X_4$ receptor mRNA have been detected in PC 12 cells (Hur *et al.* 2001). P2X receptors mediate fast ionic flow and are supposed to induce depolarization of the cells, hence contributing to the catecholamine release from PC12 cells. Therefore, we first analyzed P2X receptors and their modulation by UCH L1. This is the first report to show a relationship between UCH L1 and neurotransmitter receptors and may help to understand the function of UCH L1 in the nervous system.

Materials and methods

Cell culture

PC12 Tet-off cells were grown in RPMI-1640 medium containing 5% fetal bovine serum (FBS) (Cell Culture Technologies, CANSER INTERNATIONAL INC., Canada), 10% horse serum (HS) (Gibco/BRL, Grand Island, NY, USA), 100 units/mL penicillin (Life Technologies, Rockville, MD, USA) and 100 μg/mL streptomycin (Life Technologies) in a humidified atmosphere with 10% CO_2 at 37°C. To differentiate PC12 Tet-off cells, 100 ng/mL of nerve growth factor (NGF) was added to the RPM1640 medium with 0.1% HS, 0.05% FBS, 50 unit/mL penicillin and 100 μg/mL streptomycin for 4 days.

CHO-AA8-Lucl cells were maintained in Minimum Essential Medium Eagle α modification (Sigma, St Louis, MO, USA) containing 10% FBS, 100 units/mL penicillin, 100 μg/mL streptomycin, and 4 mM L-glutamine (Gibco/BRL), with 10% CO_2 at 37°C.

Transfection

Plasmids used for transfection were constructed using pBI-EGFP Tet vector (Clontech). For electrophysiological recording, PC12 Tet-Off cells were transfected with mock, wild-type or mutant (C90S) human UCH L1 cDNA, using Lipofectamine 2000. After 24 h, PC12 Tet-Off cells were treated with NGF and differentiated for 4–5 days. More precisely, $3.0 \times \sim 10^5$/dish PC12 Tet-Off cells were seeded in 35-mm dishes in RPMI with 10% HS and 5% FBS. Twenty-four hours after seeding, the medium was replaced with 500 μL of serum-free RPMI1640 medium. Then, the transfection mixture containing 4 μg of cDNA and 10 μL of Lipofectamine 2000 in 500 μL of RPMI-1640 was added to each dish and incubated for 6 h in a humidified atmosphere with 10% CO_2 at 37°C. One ml of complete RPMI-1640 supplemented with an additional 10% HS and 5% FBS was then added to each dish. The solution for transfection was discarded 18 h later and replaced with RPMI-1640 medium for differentiation with added 100 ng/mL NGF. For protein analysis, CHO-AA8-Lucl cells ($7.5 \times \sim 10^5$/well, Clontech) were transfected in the same way. After 24 h, cells were subjected to western blot analysis or immunocytochemical analysis.

Western blot analysis

Transfected CHO-AA8-Lucl cells were washed with PBS contained protease inhibitor and after collecting lysates in solution containing 20 mM Tris-base, 0.1% SDS, 1% sodium deoxycholate, 1% Triton X-100 and 0.001 g/5 mL protease inhibitor and then centrifuged at 15 000 r.p.m. for 30 min at 4°C. After collecting supernatant, protein concentrations of lysates were determined using Bio-Rad protein assay kits (Bio-Rad, Hercules, CA, USA). Lysates were boiled for 10 min, resolved by 10–20% gradient SDS-PAGE, and transferred to polyvinylidene difluoride membranes (Bio-Rad) with a semidry electroblotter (Bio-Rad). The membrane was blocked by incubation in 1% BSA/TBST for 1 h at room temperature. Anti-PGP9.5 (UCH L1) antibody (1 : 100, Medac) was used as a primary antibody in Western blotting. Anti-rabbit IgG conjugated with

horseradish peroxidase (1: 2000) (Dako, Carpinteria, CA, USA) was used as secondary antibody. Immunoreactive bands were detected using the supersignal substrate system (Pierce, Rockford, IL, USA) according to manufacturer's instructions.

Immunocytochemical analysis

After transfection, cells were fixed with 4% paraformaldehyde. Immunocytochemistry on CHO-AA8-Lucl cells and PC12 Tet-Off cells was performed as previously described (Osaka *et al.* 2003) using antibodies to ubiquitin that is predominantly reactive to free ubiuitin in immuno-histochemistry (1 : 100, Sigma; polyclonal) and UCH L1 (1 : 100, Medac; monoclonal). For immunofluorescence studies, antirabbit IgG conjugated with Cy3 antibodies (1 : 200, Jackson Immuno Research) and antirabbit IgG conjugated with Alexa Fluor 568 antibodies (1 : 1000, Molecular Probes) were used as secondary antibodies. Also, in PC12 Tet-Off cells, 300 μM DAPI was applied to stain transfected and untransfected cell nuclei for 5 min, and then the cells were washed with PBS for 5 min at least five times. Twenty confocal images with 0.5 μm width were obtained and reconstructed using the confocal laser microscope system (Radiance2100, Bio-Rad). To stain mono-ubiquitin, the same laser strength was used in mock, wild-type and C90S UCH L1-transfeacted cells under the confocal laser microscope system (LSM510, Carl Zeiss, Germany).

Electrophysiological measurements

The cell with fluorescence was chosen under the fluorescence microscope. Then, the patch pipette was applied to the cell to obtain a giga-ohm seal under the phase bright mode. Whole-cell recordings were made as reported previously (Noda *et al.* 1999, 2000), using an Axopatch-200B amplifier (Axon Instruments, Foster City, CA, USA), under voltage-clamp condition at the holding potential of −70 mV. Membrane currents were measured using a patch pipette containing (in mM): CsCl, 120; Mg_2ATP_3, 3; HEPES, 20; $CaCl_2$, 1; $MgCl_2$, 1; EGTA, 5. The pH of the solution was adjusted to 7.2 with 1 N CsOH. The pipette resistance was 5–9 MΩ. The external solution contained (mM): NaCl, 132; KCl, 5; $CaCl_2$, 2; $MgCl_2$, 1; glucose, 10; and HEPES, 10. The pH was adjusted to 7.4 with 1 N NaOH. External ATP or drugs were applied rapidly using the 'Y tube' technique (Min *et al.* 1996), which allows the complete exchange of the external solution surrounding a cell within 20 ms. Temperature monitored in the recording dishes was 33–34°C.

In the experiments using inhibitors except PD98059, ATP was applied twice to ensure reproducibility of the ATP-induced current in control experiments. The inhibitor solution was applied after first application of ATP for the period according to the references for each inhibitor until the end of second application of ATP. The current amplitude obtained at the second application of ATP with or without inhibitors normalized to the first ATP-induced current. All values were presented as means ± SEM. Statistical analysis was done using ANOVA. A value of $p < 0.05$ was considered to be the minimum level of significance. Curve fitting was performed using Hill Equation (Igor Pro 4.07; Wavemetrics, Lake Oswego, OR, USA).

SYBR Green-based Real-Time Quantitative RT–PCR

Total RNAs were prepared from 2×10^6 PC12 Tet-Off cells and a rat brain with RNeasy™. RNA purification kit (QIAGEN, Valencia, CA, USA) according to the manufacturer's protocol. First-strand cDNA synthesized from 1 μg total RNA with random hexamer primers was used as template for each reaction. SYBR Green-based Real-time Quantitative RT-PCR was performed as described (Wong *et al.* 2000; Aoki *et al.* 2002). Applied Biosystems 7700 Sequence Detection System was used for the signal detection and the PCR was performed in 1 × SYBR Green Master mix (Applied Biosystems, Foster City, CA, USA) and 50 nM of each primer. For standardization and quantification, rat β-actin or rat glyceraldehyde 3-phosphate dehydrogenase (GAPDH) was amplified simultaneously. Primer sequences were designed with Primer Express™. Software (Applied Biosystems). The following primer pairs were employed: 5′-TGCAGACCATCAGCAACCTG-3′ (upper, 17–36) and 5′-CTTGTGGATACCCCAGCTCC-3′ (lower, 103–84) for amplification of rat DARPP-32 (primer set A; GenBank accession No. AF281661): 5′-CACCTGCAGACCATCAGCAA-3′ (upper, 13–32) and 5′-CCTCTTGTGGATACCCCAGC-3′ (lower, 106–87) for amplification of rat DARPP-32 (primer set B; AF281661): 5′- ATCGCTGACAGGATGCAGAAG-3′ (upper, 925–945) and 5′-AGAGCCACCAATCCACACAGA-3′ (lower, 1032–1012) for amplification of rat β-actin: and 5′-ACCACAGTCCATGCCATCAC-3′ (upper, 586–605) and 5′- TCCACCACCCTGTTGCTGTA-3′ (lower, 1037–1018) for amplification of rat GAPDH. PCR conditions were: 95°C for 10 min, followed by 40 cycles at 95°C for 15 s and 60°C for 1 min. The threshold cycle of each gene was determined as the PCR cycle at which an increase in fluorescence was observed above the baseline signal in an amplification plot (Wada *et al.* 2000). The 'normalized expression level of target' (dCt) was calculated as the difference in threshold cycles for target and reference (β-actin or GAPDH). Subtraction of dCt for PC12 Tet-Off cells from dCt for the rat brain provided the ddCt value. The formula, 2^{-ddCt}, was used to calculate relative expression levels for PC12 Tet-Off cells compared to the rat brain. To reduce possible error, RT-PCR reaction was performed three times and averaged 2^{-ddCt} values were obtained. In addition, two gene-specific primer sets (set A and B, see above) for DARPP-32 gene and two independent RNA pools were examined to confirm DARPP-32 gene expression.

Drugs and reagents

RPMI-1640 medium, ATP-2Na, H-89, chelerythrine, roscovitine, PD98059, forskolin and 1,9-dideoxyforskolin were from SIGMA (St. Louis, MO, USA). NGF and Lipofectamine 2000 were from Gibco/BRL (Grand Island, NY, USA). KN-93 and okadaic acid was from CALBIOCHEM (San Diego, CA, USA).

Results

Transfection of UCH L1 in PC12 Tet-Off cells

Expression activity of plasmid constructs was first examined in CHO-AA8-Lucl cells that lack endogenous expression of UCH L1 (Fig. 1). Confocal microscopic examination revealed that UCH L1 immunoreactivity colocalizes with GFP fluorescence (Fig. 1a). Western blot analysis showed bands immunostained by anti-UCH L1 antibodies were

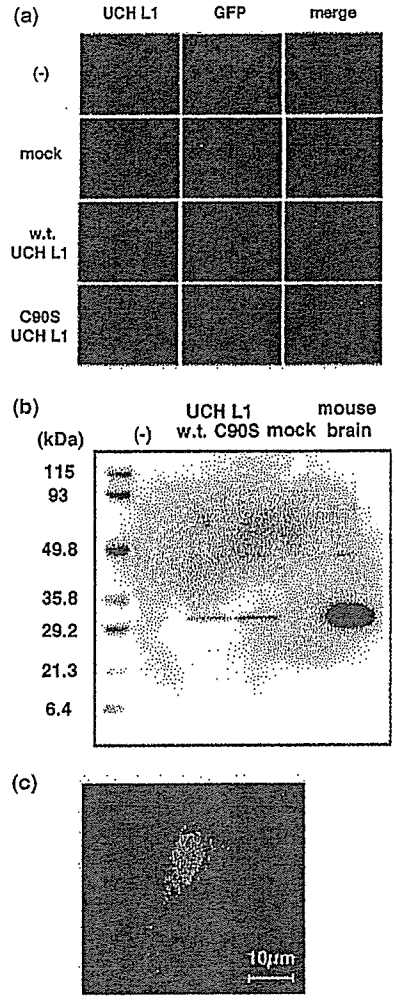

Fig. 1 Transfection efficacy of UCH L1 in CHO-AA8-LucI cells and PC12 Tet-Off cells. (a) Confocal image of CHO-AA8-LucI cells 24 h after transfection of pBI-EGFP-mock, wild type UCH L1 and C90S UCH L1 with Lipofectamine 2000 were double stained with UCH L1 (red). Cells with green fluorescence (GFP) are the transfected cells. (b) Western-blot analysis of CHO-AA8-LucI cells 24 h after transfection of pBI-EGFP-mock, -wild type UCH L1 and -C90S UCH L1 with Lipofectamine 2000. CHO-AA8-LucI cells were lysed with TBS buffer containing 0.1% Triton X. 10 μg of each protein was subjected to SDS-PAGE and immunoblotted with anti-PGP9.5 antibody. (c) Confocal image of overexpressed UCH L1 in PC12 Tet-Off cells were double stained with GFP (green) and DAPI (blue).

detected in cells transfected with pBI-EGFP-wild type UCH L1 or C90S UCH L1, but not mock plasmids (Fig. 1b). Figure 1(c) shows a PC12 Tet-Off representative cell with green fluorescence used for electrophysiological recording, although DAPI staining was not employed for the recording. The efficacy of the transfection was about 10% in PC12 Tet-Off cells.

Effects of overexpression of UCH L1 on ATP-induced currents

ATP-activated inward currents due to the activation of P2X receptors at the negative holding potential in PC12 cells were reported (Nakazawa *et al.* 1994). In our experiments, PC12 Tet-Off cells were voltage clamped at −70 mV and high concentration of ATP were used to see whether or not overexpression of UCH L1 affected maximum inward currents. In UCH L1-transfected PC12 Tet-Off cells, ATP-induced inward currents were significantly larger than those in mock-transfected cells. Unexpectedly the mutant (C90S) UCH L1, which lacks C-terminal hydrolase activity but retains ubiquitin binding affinity, had a similar effect to wild-type UCH L1 (Fig. 2a). The amplitude of peak inward currents in mock-, wild-type UCH L1- and C90S UCH L1-transfected PC12 Tet-Off cells were 15.0 ± 1.6 pA/pF ($n = 5$), 48.5 ± 6.0 pA/pF ($n = 6$) and 47.6 ± 4.1 pA/pF ($n = 6$), respectively (Fig. 2b).

The current-voltage relationships of ATP-induced inward currents were analyzed by applying voltage steps of 10 mV increments between −100 mV and + 50 mV with 50 ms duration and 50 ms interval from the holding potential of −70 mV before and during the application of ATP (Fig. 3a). The current traces before and after application of ATP in wild-type UCH L1-transfected PC12 Tet-Off cells were shown by applying voltage steps (Fig. 3b). Holding currents were negligibly misaligned even during the application of ATP. The current levels at the end of each pulse before and during ATP application were obtained in mock-, wild-type UCH L1- or C90S UCH L1-transfected PC12 Tet-Off cells.

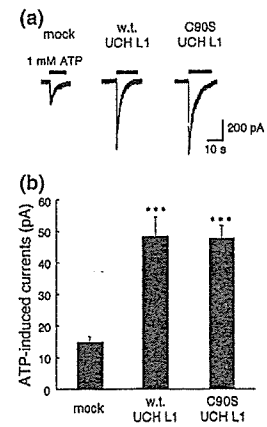

Fig. 2 Current amplitudes of ATP-induced currents in mock-, wild-type UCH L1- and C90S UCH L1-transfected PC12 Tet-Off cells. (a) Inward membrane currents induced by 1 mM ATP at the holding potential of −70 mV in mock-, wild-type (wt) and C90S UCH L1-transfected PC12 Tet-Off cells. (b) Amplitudes of peak inward currents induced by 1 mM ATP in mock-, wild-type and C90S UCH L1-transfected PC12 Tet-Off cells. The bars represent the mean ± SEM. ***: $p < 0.001$.

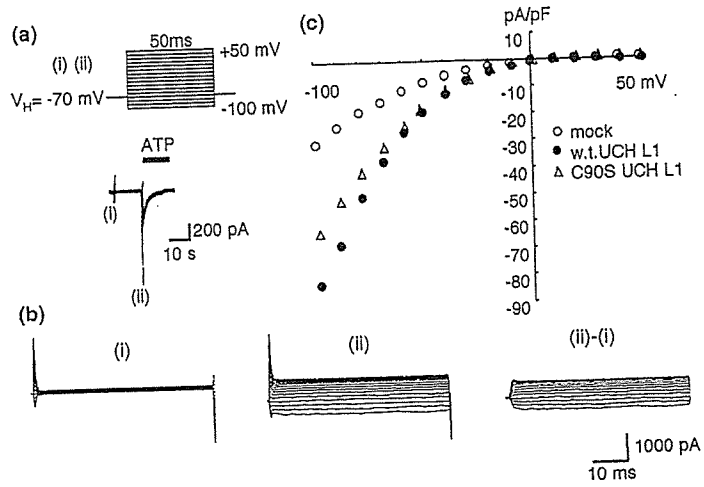

Fig. 3 Voltage-dependency of ATP-induced currents in mock-, wild-type UCH L1- and C90S UCH L1-transfected PC12 Tet-Off cells. A: The voltage protocol shown in the upper panel was applied before and during application of 1 mM ATP at the time indicated by (i) and (ii) in the lower panel. (b) Cumulated current traces obtained in wild type UCH L1-transfected cells before (i) and during (ii) application of ATP. The subtracted current traces [(i)-(ii)] show the ATP-induced currents. (c) The current–voltage relationships of ATP-induced currents. The amplitudes of subtracted currents [(ii)-(I)] in (b) at the end of 50 ms pulses were plotted against the pulse potentials in mock- (O), wild-type (●) and C90S UCH L1-transfected cells (△).

Then the amplitudes of ATP-induced currents at different voltages were obtained by subtracting the one before application of ATP from the one during application of ATP, and were plotted as in Fig. 3(c). In consideration of desensitization, the current-voltage relationships were obtained by applying voltage steps in opposite direction, i.e. from + 50 to − 100 mV, but there was almost no change (data not shown). The reversal potential was about 0 mV, suggesting that these currents were due to non-specific cationic channels.

ATP-induced inward currents were concentration dependent and the sensitivity of ATP was not significantly changed by overexpression of either wild- or C90S UCH L1. Each EC_{50} was 34 μM, 40 μM and 62 μM and each Hill coefficient (n_H) was 1.38, 1.48 and 1.34 in mock-, wild-type and C90S UCH L1-transfected cells, respectively (Fig. 4).

Effects of wild type and C90S UCH L1 on mono-ubiquitin expression

It was reported that absence of UCH L1 reduced the mono-ubiquitin level in mouse brain and UCH L1 overexpression increased the level of mono-ubiquitin by alteration of ubiquitin metabolism in cultured cells. Therefore, UCH L1-mediated increases in ubiquitin levels are a function of UCH L1 affinity for ubiquitin rather than hydrolase activity (Osaka *et al.* 2003). To clarify the effect of UCH L1 on ubiquitin levels in PC12 Tet-Off cells, ubiquitin was visualized using confocal immunofluorescence microscopy (Fig. 5). Wild-type UCH L1-transfected cells showed stronger immunoreactivity for ubiquitin compared with those in mock-transfected cells or non-transfected cells in the same field. Increased ubiquitin immunoreactivity was also evident in C90S UCH L1-transfected cells. These results were consistent with the previous report that ubiquitin were up-regulated by UCH L1 (Osaka *et al.* 2003).

Effects of Kinase inhibitors on ATP-induced currents in UCH L1-transfected cells

The mechanism by which ATP-induced currents were augmented in UCH L1-transfected cells was investigated. It was reported that in *Aplysia* UCH activated PKA as a result of the degradation of regulatory subunit of PKA, which contributed the long-term potentiation (Hegde *et al.* 1997). Therefore, the possibility of the involvement of the activated PKA was tested by using H-89, a PKA inhibitor. After obtaining a large ATP-induced currents in the UCH L1-transfected cells, 10 μM H-89 was applied for 10 min. The amplitude of ATP-induced currents in the presence of H-89 was 48.1 ± 3.51% (n = 8) compared to the first ATP-induced current in the same cell (control without H-89; 71.2 ± 5.6% (n = 7)) (Fig. 6a). Also, it was reported that the intracellular carboxyl terminus of P2X receptor contains several consensus phosphorylation sites for PKC as well as PKA, suggesting that the function of the P2X receptor could be regulated by protein phosphorylation (Chow and Wang 1998). Hence, the possibility of the involvement of the activated PKC was tested by using chelerythrine, a PKC inhibitor. Application of 5 μM chelerythrine for 10 min had no effect on the ATP-induced inward current in the UCH L1-transfected cell. The relative amplitude of second

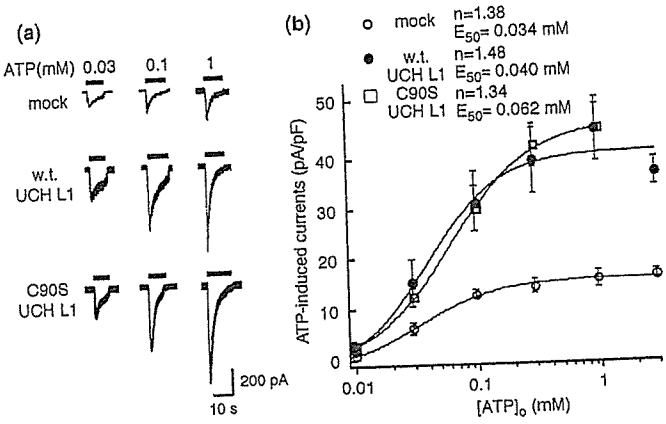

Fig. 4 Concentration-dependent curve of ATP-induced currents in mock-, wild-type and UCH L1-transfected PC12 Tet-Off cells. (a) Inward membrane currents induced by 0.03, 0.1 and 1 mM ATP at the holding potential of −70 mV in mock-, wild-type and C90S UCH L1-transfected PC12 Tet-Off cells. (b) The peak inward current induced by ATP at the holding potential of −70 mV was plotted against the ATP concentration between 0.01 and 3 mM in mock (○)-, wild-type (●) and C90S UCH L1 (□)-transfected PC12 Tet-Off cells. Each point represents the mean of five or six cells and the bar shows ± SEM. The curve shows the least squares fit, where n_H = Hill coefficient and EC_{50} = the half maximum concentration.

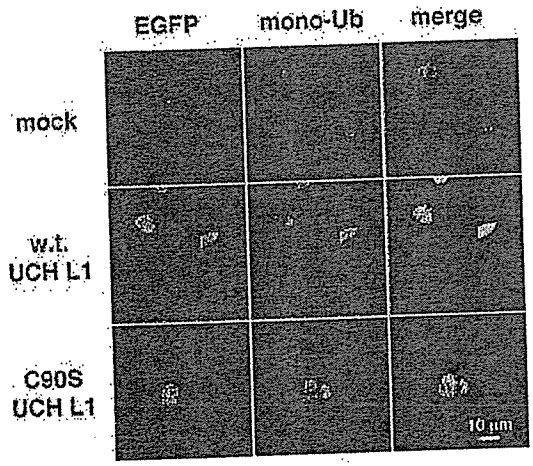

Fig. 5 Effects of wild-type and C90S UCH L1 on mono-ubiquitin expression. Confocal image of PC12 Tet-Off cells transfected pBI-EGFP-mock, wild-type (wt) UCH L1 and C90S UCH L1 with Lipofectamine 2000 were double stained with mono-ubiquitin (red) and GFP (green).

ATP-induced inward currents in the presence of chelerythrine was 71.9 ± 4.2% ($n = 7$) (control without chelerythrine; 71.2 ± 5.6% ($n = 7$)) (Fig. 6a). Furthermore, the possibility of the involvement of CaMKII was also tested by using KN-93, a CaMKII inhibitor. Application of 10 μM KN-93 for 20 min significantly reduced the ATP-induced inward current in the UCH L1-transfected cell (69.9 ± 6.7% ($n = 5$); control, 90.2 ± 3.5% ($n = 5$)) (Fig. 6b).

In UCH L1-transfected PC12 Tet-Off cells, increased ATP-induced currents were not completely reversed by H-89 or KN-93, suggesting that both PKA and CaKII contributed independently. Hence, the combination of PKA and CaMKII was tested to see whether coapplication of H-89 and KN-93 inhibited the effect of UCH L1 additively. Coapplication of 10 μM KN-93 and 10 μM H-89 attenuated ATP-induced currents more strongly than that with single kinase inhibitor. The relative amplitude of ATP-induced inward currents was 45.8 ± 2.7% ($n = 7$) (control without inhibitors; 90.2 ± 3.5% ($n = 5$)) (Fig. 6b).

In PC12 cells and hippocampal neurons, it was reported that activation of PKA caused activation of extracellular signal-regulated kinase (ERK), subsequent phosphorylation of Ca^{2+}-stimulated cAMP response element binding protein (CREB) and stimulated transcription. Such signal transduction was predicted to contribute to long-term potentiation (Impey *et al.* 1998). Likewise, the augmentation of ATP response in UCH L1-transfected cell might be due to the stimulation of transcription that increased the number of P2X receptors. To test this possibility, we examined whether mitogen-activated protein kinase (MAPK) including ERK was activated following the activation of PKA in PC12 Tet-Off cells. The result was that even after application of cells with 5 μM PD98059, one of the MAPK kinase inhibitors, for 4 days, ATP-induced currents in UCH L1-transfected cells were not affected. The amplitude of ATP-induced inward currents after the application of PD98059 was 53.3 ± 3.5 pA/pF ($n = 2$) (control without PD98059; 50.8 ± 5.2 pA/pF ($n = 8$)) (Fig. 6c).

Expression of DARPP-32 in PC12 Tet-Off cells

In rat striatum, positive feedback mechanism of dopamine signaling via PKA was reported. Activation of PKA causes phosphorylation at threonine 34 (Thr-34) of dopamine and cAMP-regulated phosphoprotein with molecular weight of

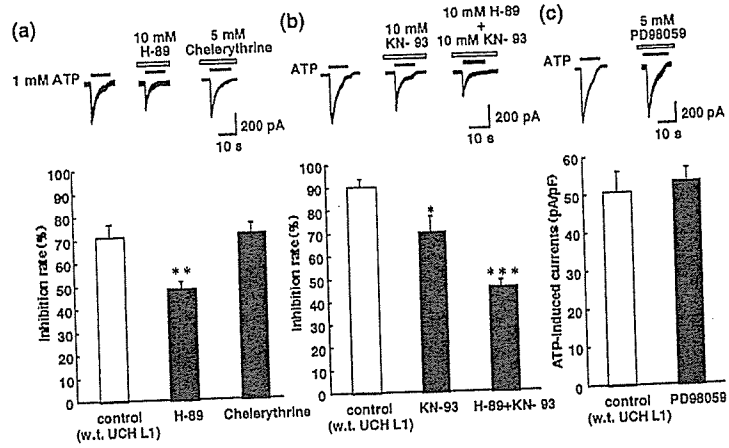

Fig. 6 Inhibition of ATP-induced currents by kinase inhibitors in wild type UCH L1-transfected PC12 Tet-Off cells. (a) ATP-induced currents were attenuated by pre-application of 10 μM H-89, a PKA inhibitor, but not by 5 μM chelerythrine, a PKC inhibitor, for 10 min. (b) ATP-induced currents were attenuated by pre-application of 10 μM KN-93, a CaMKII inhibitor, for 20 min. ATP-induced currents were further attenuated by copreapplication of 10 μM KN-93 and 10 μM H-89. C: ATP-induced currents were not affected by application of 5 μM PD98059, a MAPKK inhibitor, for four days. $^{*}p < 0.05$, $^{**}p < 0.01$, $^{***}p < 0.001$.

about 32 000 (DARPP-32), which reduces PP1 activity and consequently inhibits dephosphorylation of various substrates in the cell. On the other hand, activation of PKA stimulates PP2A activity and suppresses the phosphorylation at Thr-75 of DARPP-32. Since phosphorylation of DARPP-32 at Thr-75 has negative feedback regulation on PKA activity, dephosphorylation at Thr-75 reduces the inhibition of PKA activity (Nishi *et al.* 2000). To examine whether the similar mechanism exists in PC12 Tet-Off cells, we analyzed the expression of DARPP-32 first. With RT-PCR method using two kinds of primer sets specific to DARPP-32 (primer set A and B), the relative expression levels of DARPP-32 in rat whole brain and PC12 Tet-Off cells under non-differentiated and differentiated conditions were compared. As shown in Fig. 7(a), DARPP-32 was expressed in PC12 Tet-Off cells and the expression level tended to increase after differentiation of the cells with NGF. The possibility of the involvement of DARPP-32 and its phosphorylation was further tested using okadaic acid, a PP1 and PP2A inhibitor. The relative amplitudes of ATP-induced inward currents after the application of 100 nM okadaic acid for 20 min was significantly inhibited to $49.9 \pm 11.1\%$ ($n = 5$) (control without okadaic acid; $90.2 \pm 3.5\%$ ($n = 5$)), presumably due to the inhibition of PP2A and subsequent dephosphorylation of Thr-75, leading the release of negative feedback on PKA (Fig. 7b). Since phosphorylation of Thr-75 was also

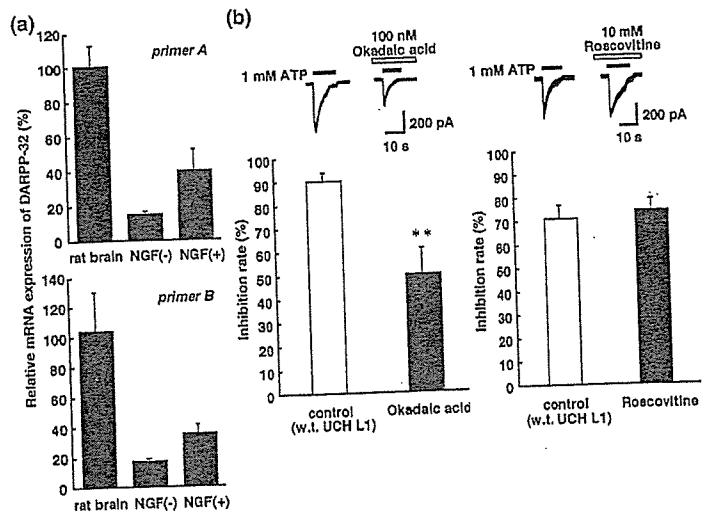

Fig. 7 Quantitative RT–PCR of DARPP-32 and effects of okadaic acid and roscovitine on ATP-induced currents in wild-type UCH L1-transfected PC12 Tet-Off cells. (a) The expression level of DARPP-32 mRNA was normalized to that of rat brain β-actin mRNA. Using two kinds of primer (a and b), PC12 Tet-Off cells were shown to express DARPP-32 whose level was increased by differentiation of the cells with NGF. B: ATP-induced currents were attenuated by preapplication of 100 nM okadaic acid, a PP1 and PP2 inhibitor, for 20 min. (c) ATP-induced currents were not affected by pre-application 10 μM roscovitine, a CDK5 inhibitor, for 10 min $^{**}p < 0.01$.

mediated by cycline-dependent kinase (CDK), the effect of a CDK inhibitor was tested to see if ATP-induced currents were more enhanced. However, application of 10 μM roscovitine for 10 min did not have significant effect (74.4 ± 5.1% (n = 4); control; 71.2 ± 5.6% (n = 7)) (Fig. 7c).

ATP-induced currents in mock-transfected cells

We concluded that the increase of ATP-induced inward currents in UCH L1-transfected cells was partly attributed to the activation of PKA. Hence, we tested whether ATP-induced currents in the cells not transfected with UCH L1 were increased by the application of forskolin, an adenylate cyclase activator that increases intracellular level of cAMP (Conn *et al.* 1989). The ATP-induced currents in mock-transfected cells were significantly increased after the application of 10 μM forskolin for 10 min (109.2 ± 2.2% (n = 5); control without forskolin; 87.4 ± 3.8% (n = 5)) (Fig. 8a). It was confirmed that application of inactive analogue of forskolin, 10 μM 1,9-dideoxyforskolin, did not have such effect (79.2 ± 2.2% (n = 5); control; 87.4 ± 3.8% (n = 5)) (Fig. 8a). Next, the effects of kinase inhibitors on ATP-induced currents were tested in mock-transfected cells. In mock-transfected cells, application of 10 μM H-89 for 10 min or 10 μM roscovitine for 10 min had no effect on the ATP-induced inward current (H-89, 84.3 ± 3.0% (n = 4); roscovitine, 93.4 ± 5.0% (n = 4); control; 87.4 ± 3.8% (n = 5)) (Fig. 8a). On the other hand, ATP-induced inward currents were significantly increased after application of 100 nM okadaic acid for 20 min (62.5 ± 6.7% (n = 5)). However, application of 10 μM KN-93 had no effect (111.3 ± 7.1% (n = 3); control; 79.0 ± 3.8% (n = 5)) (Fig. 8b).

ATP-induced currents in C90S UCH L1-transfected cells

Since ATP-induced currents in and C90S UCH L1-transfected PC12 Tet-Off cells were significantly potentiated as well, the same pharmacological analyses were done to see whether or not the mechanism was the same as in wild-type UCH L1-transfected cells. Application of 10 μM H-89 for 10 min significantly reduced ATP-induced currents in C90S UCH L1-transfected cells (61.9 ± 2.0% (n = 8); control without H-89, 78.4 ± 3.3% (n = 4)) (Fig. 9a). Also, applications of 10 μM KN-93 or 100 nM okadaic acid for 20 min significantly reduced ATP-induced inward currents in C90S UCH L1-transfected cells (KN-93, 58.0 ± 3.7% (n = 5); okadaic acid, 65.1 ± 4.9% (n = 6); control; 88.0 ± 3.4% (n = 5)) (Fig. 9b). Furthermore, ATP-induced currents were more attenuated by copreapplication of 10 μM KN-93 and 10 μM H-89 (44.2 ± 3.7% (n = 6); control; 88.0 ± 3.4% (n = 5)) (Fig. 9b).

Discussion

To analyze the functional role of UCH L1 in the central nervous system (CNS), it is important to know whether UCH L1 has any effects on ion channels and receptors that are the basic elements of neurotransmission. There are many ways to analyze them, but one of the most simple but efficient ways to start is to analyze the effects of exogenous UCH L1 in neuronal cultured cell line. To confirm that cells express the transfected protein, we used CHO-AA8-Lucl cells because of the higher transfection efficacy and not having endogenous UCH L1 (Fig. 1). For functional analyses of UCH L1 in nervous system, we used PC12 Tet-Off cells. The engineered PC12 cells are constructed to have higher transfection efficiency than wild-type PC12 cells which are one of the popular neuronal cell line (unpublished data). Among neurotransmitter receptors in PC12 cells, we analyzed ATP-activated receptors that are widely distributed in the brain and involved in various biological activities including neurosecretion. In PC12 cells, $P2X_2$ and $P2X_4$ receptors (Hur *et al.* 2001) with lower level of $P2X_6$ (unpublished data) are expressed and ATP-induced inward currents were well characterized (Nakazawa *et al.* 1994). We recorded

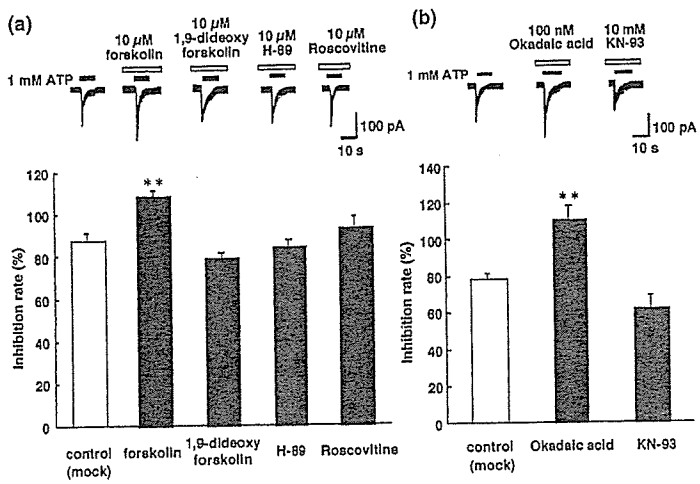

Fig. 8 ATP-induced currents in mock-transfected PC12 Tet-Off cells. (a) ATP-induced currents were augmented by preapplication of 10 μM forskolin for 10 min, but were not affected by 10 μM H-89 and 10 μM roscovitine. (b) ATP-induced currents were augmented by 100 nM okadaic acid, but were not affected by 10 μM KN-93. $^{**}p < 0.01$.

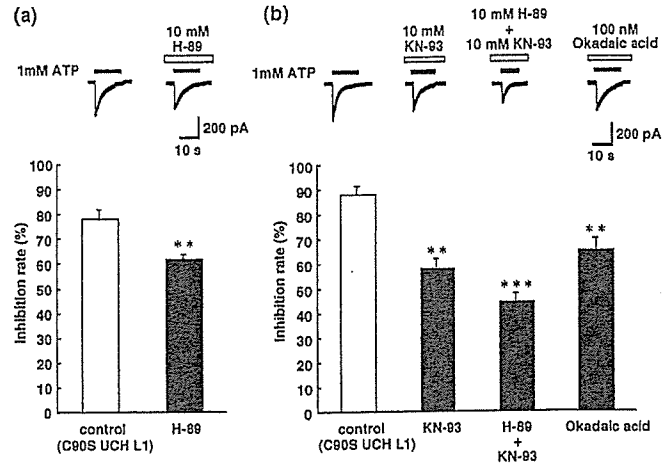

Fig. 9 ATP-induced currents in C90S UCH L1-transfected PC12 Tet-Off cells were also dependent on PKA and CaMKII. (a) ATP-induced currents were attenuated by pre-application of 10 μM H-89 for 10 min. (b) ATP-induced currents were attenuated by preapplication of 10 μM KN-93 and 100 nM okadaic acid for 20 min. ATP-induced currents were further attenuated by copreapplication of 10 μM H-89 and 10 μM KN-93. $^{**}p < 0.01$, $^{***}p < 0.001$.

ATP-induced inward currents due to the activation of P2X receptor channels at the holding potential of −70 mV under the conventional whole-cell patch clamp configuration. To analyze the effects of overexpression of UCH L1 and for pharmacological characterization, high concentration of ATP (1 mM) was used to see the effects on the maximum response to ATP. As to the possibility to analyze other receptor channels expressed in PC12 cells, nicotinic acetylcholine receptor (nAChR) was likely to be analyzed. However, no currents were recorded using ACh or nicotine (not shown), probably because nAChR required longer time to be expressed after differentiation (Fukukawa *et al.* 1992).

The amplitude of ATP-induced inward currents was significantly greater in both wild-type and mutant (C90S) UCH L1-transfected PC12 Tet-Off cells (Fig. 2a). We found that the potentiation of ATP-induced currents was due to the activation of PKA and CaMKII (Fig. 6). Though activation of PKA by homologous UCH was reported in *Aplysia* (Hegde *et al.* 1997), the mechanism of PKA activation in PC12 cells would be different from the one in *Aplysia*. In *Aplysia*, UCH enhances the degradation of the regulatory subunit of PKA and consequently activate PKA. However, in our study, the mutant (C90S) UCH L1, which lacks hydrolase activity, also potentiated ATP-induced currents, which was also attenuated by H-89 and KN-93 (Figs 2 and 9). Therefore, function of UCH L1 other than hydrolase activity should play a fundamental role. Based on the previous reports that UCH L1 has multifunction, one of the plausible reason would be the ability to increase free ubiquitin by both wild-type and C90S mutant UCH L1. It was reported that C90S UCH L1 lacks hydrolase activity, but retains ubiquitin binding affinity and increases free ubiquitin level in SH-SY5Y cells (Osaka *et al.* 2003). Actually, immunostaining of mono-ubiquitin was stronger in the cytoplasm of wild-type and C90S UCH L1-transfected PC12 Tet-Off cells (Fig. 5). The mechanism how increased level of mono-ubiquitin activated PKA and CaMKII were not yet known and should be investigated further.

The mechanism how activated PKA and CaMKII potentiate ATP-induced currents also remains to be investigated. One possible mechanism would be phosphorylation of P2X receptors by these protein kinases, though it was reported that activation of PKA reduced the magnitude of the ATP-activated current in $P2X_2$-transfected HEK293 cells (Chow and Wang 1998). The potentiation of ATP-induced currents by PKA in our study might be similar to the one observed for Ca^{2+} channels (Kamp and Hell 2000). Likewise, in mock-transfected cells, the amplitude of ATP-induced currents was significantly increased by forskolin, an adenylate cyclase activator that increases intracellular levels of cAMP and activates PKA (Fig. 8). Therefore, it was suggested that at least an activation of PKA contributed to the potentiation of ATP-induced currents. As for the involvement of CaMKII, it has been recently reported that CaMKII potentiates ATP responses by promoting trafficking of P2X receptors (Xu and Huang 2004), suggesting that phosphorylation of P2X receptors were not the sole mechanism of the potentiation of ATP-induced currents. Furthermore, since increased ATP-induced currents were not completely reduced by H-89, KN-93 nor coapplication of H-89 and KN-93 in wild-type or C90S UCH L1-transfected cells (Figs 6 and 9), it was also suggested that activation of PKA and CaMKII was not the sole mechanism of the potentiation of ATP-induced currents but there may be other components, too.

Another possible mechanism how PKA potentiates ATP-induced currents would be an increase in number of P2X receptors. In *Aplysia*, homologous UCH activates PKA and consequently activates MAPK and subsequent transcription (Hegde *et al.* 1997). Such signal transduction is predicted to contribute to a long-term potentiation (Impey *et al.* 1998). If the similar signaling exists in mammalian cells, the number of P2X receptors could increase during the differentiation

after transfection of UCH L1 or C90S UCH L1. However, it was unlikely because even after incubation with MAPK inhibitor during differentiation, the augmented ATP-induced currents were still observed in wild-type (Fig. 6c) or C90S UCH L1-transfected cells (not shown).

There may be indirect effects of phosphorylation by PKA on P2X receptors. In rat striatum, it has been suggested that there are positive and negative feedback system of DARPP-32 via activation of PKA and CDK5, respectively (Nishi *et al.* 2000). To test whether the similar mechanism exists in PC12 Tet-Off cells, we first analyzed the expression of DARPP-32 with RT-PCR. DARPP-32 was expressed in PC12 Tet-Off cells and we found that the expression level of DARPP-32 was increased after differentiation of the cells with NGF (Fig. 7). Thus, the possibility of the involvement of DARPP-32 in the P2X receptor activation was tested with using okadaic acid, a PP1 and PP2A inhibitor, and roscovitine, a CDK5 inhibitor. Roscovitine had no effects on the ATP-induced currents in mock- and UCH L1-transfected PC12 Tet-Off cells, suggesting that CDK5 did not play an important role in the regulation of P2X receptor via DARPP-32 in PC12 Tet-Off cells. On the other hand, the ATP-induced inward currents were attenuated by okadaic acid in wild-type or C90S UCH L1-transfected PC12 Tet-Off cells (Figs 7b and 9b), but increased in mock-transfected PC12 Tet-Off cells (Fig. 8b). Based on these results, we assume the followings; (1) In wild-type and C90S UCH L1-transfected cells, activation of PKA by wild-type or C90S UCH L1 stimulates PP2A activity and dephosphorylate DARPP-32 at Thr-75. Since phosphorylation of DARPP-32 at Thr-75 inhibits PKA activity, inhibition of PP2A by okadaic acid accelerates phosphorylation at Thr-75, which in turn has a negative feedback effect on PKA activity and their substrates. On the other hand, activation of PKA by wild-type or C90S UCH L1 causes phosphorylation at Thr-34 of DARPP-32, which in turn reduces PP1 activity. If PP1 activity is already low enough, okadaic acid does not have significant effect on dephosphorylation of P2X receptors and presumably other proteins by PP1 (Fig. 10, *right*). (2) In mock-transfected PC12 Tet-Off cells, PKA activity is supposed to be low, because H-89 did not have significant effect and forskolin augmented the ATP-induced currents (Fig. 8a). Under this condition, PP1 activity might be prominent, which dephosphorylates various substrates including P2X receptors. Without activation of PKA, less phosphorylation at Thr-34 and less activation of PP2A, which in turn cause more phosphorylation at Thr-75 (Fig. 10, *left*). Therefore inhibition of mainly PP1 by okadaic acid could prevent the dephosphorylation of P2X receptor, increasing ATP-induced currents. (3) In both UCH L1- and mock-transfected PC12 Tet-Off cells, phosphorylation of DARPP-32 at Thr-75 by CDK5 might be negligible and CDK5 signaling did not have significant effect, unlike in neostriatal neurons (Nishi *et al.* 2000; Bibb *et al.* 2001).

As a conclusion, our present observation indicates that UCH L1 potentiates ATP responses due to activation of P2X receptors by up-regulation of ubiquitin level, activation of PKA and CaMKII, and regulation of DARPP-32. As UCH L1 has multifunction and is known to be transported over long distances via slow axonal transport to synapses (Bizzi *et al.* 1991), UCH L1 is supposed to have various effects on neuronal function. Our finding shows the first evidence that there is a relationship between UCH L1 and neurotransmitter receptor, suggesting that UCH L1 may play an important role in synaptic activity. The question whether UCH L1 can affect other neurotransmitter receptors such as GABA and glutamate receptors should be investigated further. On the contrary, ubiquitin reduction and the consequent inadequate ubiquitination of proteins may trigger accumulation of proteins that should undergo ubiquitin-dependent degradation (Wang *et al.* 2004). The question whether lack of UCH L1 interfere the functional role of neurotransmitter receptors should be

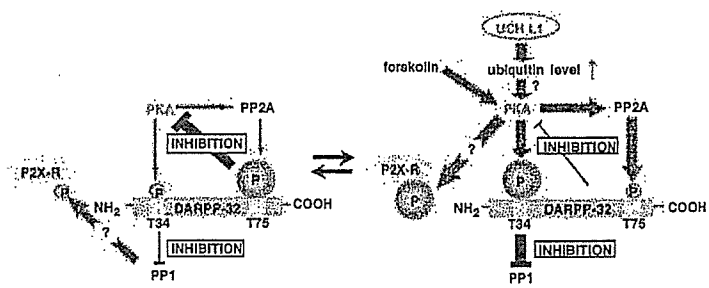

Fig. 10 Predicted PKA signaling via DARPP-32 in mock- and wild-type or C90S UCH L1 -transfected PC12 Tet-Off cells. Left: In mock-transfected cells, corresponding to basal condition, phosphorylation of DARPP-32 at Thr-75 has negative feedback effect on PKA, Down-regulation of PKA also results in less phosphorylation of DARPP-32 at Thr-34 and therefore less inhibition of PP1. Down-regulated PKA and PP1 are supposed to reduce the phosphorylation of P2X receptors. Right: In wild-type or C90S UCH L1-transfected cells, PKA is reported to activate PP2A, which dephosphorylate DARPP-32 at Thr-75, subsequently removing the negative feedback on PKA. Activation of PKA also results in the increased phosphorylation of DARPP-32 at Thr-34, which in turn inhibits PP1. Activation of PKA and inhibition of PP1 are supposed to increase the phosphorylation of P2X receptors.

investigated next. These studies may help to understand how dysfunction of UCH L1 causes neurodegeneration.

Acknowledgements

We thank Ms. Yuki Kosai for technical assistance in gaining confocal images. This work was supported by Grants-in Aid for Scientific Research of Japan Society for Promotion of Science, Grants-in Aid for Scientific Research in Priority Area Research of the Ministry of Education, Culture, Sports, Science and Technology, Japan, Kyushu University Foundation, Grants-in-Aid for Scientific Research of the Ministry of Health, Labour and Welfare, Japan and a grant from Pharmaceuticals and Medical Devices Agency, Japan.

References

Aoki K., Sun Y. J., Aoki S., Wada K. and Wada E. (2002) Cloning, expression, and mapping of a gene that is upregulated in adipose tissue of mice deficient in bombesin receptor subtype-3. *Biochem. Biophys. Res. Commun.* **290**, 1282–1288.

Bibb J. A., Chen J., Taylor J. R., Svenningsson P., Nishi A., Snyder G. L., Yan Z., Sagawa Z. K., Ouimet C. C., Nairn A. C., Nestler E. J. and Greengard P. (2001) Effects of chronic exposure to cocaine are regulated by the neuronal protein Cdk5. *Nature* **410**, 376–380.

Bizzi A., Schaetzle B., Patton A., Gambetti P. and Autilio-Gambetti L. (1991) Axonal transport of two major components of the ubiquitin system: free ubiquitin and ubiquitin carboxyl-terminal hydrolase PGP 9.5. *Brain Res.* **548**, 292–299.

Chow Y. W. and Wang H. L. (1998) Functional modulation of P2X2 receptors by cyclic AMP-dependent protein kinase. *J. Neurochem.* **70**, 2606–2612.

Ciechanover A., Orian A. and SchwartZ. A. L. (2000) The ubiquitin-mediated proteolytic pathway: Mode of action and clinical implications. *J. Cell Biochem.* **77**, 40–51.

Conn P. J., Strong J. A., Azhderian E. M., Nairn A. C., Greengard P. and Kaczmarek L. K. (1989) Protein kinase inhibitors selectively block phorbol ester- or forskolin-induced changes in excitability of Aplysia neurons. *J. Neurosci.* **9**, 473–479.

Coux O., Tanaka K. and Goldberg A. L. (1996) Structure and function of the 20S and 26S proteasomes. *Annu. Rev. Biochem.* **65**, 801–847.

Fukukawa K., Akaike M., Onodera H. and Kogure K. (1992) Expression of 5-HT3 receptor in PC12 cells treated with NGF and 8-Br.-cAMP. *J. Neurophysiol.* **67**, 812–819.

Harada T., Harada C., Wang Y. L., Osaka H., Amanai K., Tanaka K., Takizawa S., Setsuie R., Sakurai M., Sato Y., Noda M. and Wada K. (2004) Role of ubiquitin carboxy terminal hydrolase-l1 in neural cell apoptosis induced by ischemic retinal injury in vivo. *Am. J. Pathol.* **164**, 59–64.

Hegde A. N., Inokuchi K., Pei W., Casadio A., Ghirardi M., Chain D. G., Martin K. C., Kandel E. R. and SchwartZ. J. H. (1997) Ubiquitin C-terminal hydrolase is an immediate-early gene essential for long-term facilitation in Aplysia. *Cell* **89**, 115–126.

Huang Y., Baker R. T. and Fischer-Vize J. A. (1995) Control of cell fate by a deubiquitinating enzyme encoded by fat facets gene. *Science* **270**, 1828–1831.

Hur E. M., Park T. J. and Kim K. T. (2001) Coupling of l-type voltage-sensitive calcium channels to P2X (2) purinoceptors in PC-12 cells. *Am. J. Physiol. Cell Physiol.* **280**, C1121–C1129.

Ikeuchi Y., Nishizaki T., Mori M. and Okada Y. (1996) Regulation of the potassium current and cytosolic Ca^{2+} release induced by 2-methylthio ATP in hippocampal neurons. *Biochem. Biophys. Res. Commun.* **218**, 428–433.

Impey S., Obrietan K., Wong S. T., Poser S., Yano S., Wayman G., Deloulme J. C., Chan G. and Storm D. R. (1998) Cross talk between ERK and PKA is required for Ca^{2+} stimulation of CREB-dependent transcription and ERK nuclear translocation. *Neuron* **21**, 869–883.

Kamp T. J. and Hell J. W. (2000) Regulation of cardiac l-type calcium channels by protein kinase A and protein kinase C. *Circ Res.* **87**, 1095–1102.

King R. W., Deshaies R. J., Peters J.-M. and Kirschner M. W. (1996) How proteolysis drives the cell cycle. *Science* **274**, 1652–1659.

Kwon J., Wang Y. L., Setsuie R., Sekiguchi S., Sakurai M., Sato Y., Lee W. W., Ishii Y., Kyuwa S., Noda M., Wada K. and Yoshikawa Y. (2004a) Developmental regulation of ubiquitin C-terminal hydrolase isozyme expression during spermatogenesis in mice. *Biol. Reprod.* **71**, 515–521.

Kwon J., Wang Y. L., Setsuie R., Sekiguchi S., Sato Y., Sakurai M., Noda M., Aoki S., Yoshikawa Y. and Wada K. (2004b) Two closely related ubiquitin C-terminal hydrolase isozymes function as reciprocal modulators of germ cell apoptosis in cryptorchid testes. *Am. J. Pathol.* **165**, 1367–1374.

Leroy E., Boyer R., Auburger G., Leube B., Ulm G., Mezey E., Harta G., Brownstein M. J., Jonnalagada S., Chernova T., Dehejia A., Lavedan C., Gasser T., Steinbach P. J., Wilkinson K. D. and Polymeropoulos M. H. (1998) The ubiquitin pathway in Parkinson's disease. *Nature* **395**, 451–452.

Liu Y., Fallon L., Lashuel H. A., Liu Z. and Lansbury P. T. Jr (2002) The UCH-L1 gene encodes two opposing enzymatic activities that affect alpha-synuclein degradation and Parkinson's disease susceptibility. *Cell* **111**, 209–218.

Min B. I., Kim C. J., Rhee J. S. and Akaike N. (1996) Modulation of glycin-induced chloride current in acutely dissociated rat periaqueductal gray neurons by 1-opioid agonist DAGO. *Brain Res.* **734**, 72–78.

Muralidhar M. G. and Thomas J. B. (1993) The Drosophila bendless gene encodes a neural protein related to ubiquitin-conjugating enzymes. *Neuron* **11**, 253–266.

Nakazawa K., Inoue K., Koizumi S. and Inoue K. (1994) Facilitation by 5-hydroxytryptamine of ATP-activated current in rat pheochromocytoma cells. *Pflugers Arch.* **427**, 492–499.

Nishi A., Bibb J. A., Snyder G. L., Higashi H., Nairn A. C. and Greengard P. (2000) Amplification of dopaminergic signaling by a positive feedback loop. Proceedings *Natl. Acad. Sci. USA* **97**, 12 840–12 845.

Noda M., Nakanishi H. and Akaike N. (1999) Glutamate release from microglia via glutamate transporter is enhanced by amyloid-beta peptide. *Neuroscience.* **92**, 1465–1474.

Noda M., Nakanishi H., Nabekura J. and Akaike N. (2000) AMPA-KA subtypes of glutamate receptor in rat cerebral microglia. *J. Neurosci.* **20**, 251–258.

Oh C. E., McMahon R., Benzer S. and Tanouye M. A. (1994) bendless, a Drosophila gene affecting neuronal connectivity, encodes a ubiquitin-conjugating enzyme homolog. *J. Neurosci.* **14**, 3166–3179.

Osaka H., Wang Y. L., Takada K., Takizawa S., Setsuie R., Li H., Sato Y., Nishikawa K., Sun Y. J., Sakurai M., Harada T., Hara Y., Kimura I., Chiba S., Namikawa K., Kiyama H., Noda M., Aoki S. and Wada K. (2003) Ubiquitin carboxy-terminal hydrolase L1 binds to and stabilizes monoubiquitin in neuron. *Hum. Mol. Genet.* **12**, 1945–1958.

Rock K. L., Gram C., Rothstein L., Clark K., Stein R., Dick L., Hwang D. and Goldberg A. L. (1994) Inhibitors of the proteasome block the degradation of most cell proteins and the generation of peptides present on MHC class I molecules. *Cell* **78**, 761–771.

Saigoh K., Wang Y. L., Suh J. G., Yamanishi T., Sakai Y., Kiyosawa H., Harada T., Ichihara N., Wakana S., Kikuchi T. and Wada K. (1999)

Intragenic deletion in the gene encoding ubiquitin carboxy-terminal hydrolase in gad mice. *Nat. Genet.* **23**, 47–51.

Sela D., Ram E. and Atlas D. (1991) ATP receptor. A putative receptor-operated channel in PC-12 cells. *J. Biol. Chem.* **266**, 17 990–17 994.

Verma I. M., Stevenson J. K., SchwartZ. E. M., Van Antwerp D. and Miyamoto S. (1995) Rel/NF-κB/I-κB family: intimate tales of association and dissociation. *Genes Dev.* **9**, 2723–2735.

Wada R., Tifft C. J. and Proia R. L. (2000) Microglial activation precedes acute neurodegeneration in Sandhoff disease and is suppressed by bone marrow transplantation. *Proc. Natl. Acad. Sci. USA* **97**, 10 954–10 959.

Wang Y. L., Takeda A., Osaka H., Hara Y., Furuta A., Setsuie R., Sun Y. J., Kwon J., Sato Y., Sakurai M., Noda M., Yoshikawa Y. and Wada K. (2004) Accumulation of beta- and gamma-synucleins in the ubiquitin carboxyl-terminal hydrolase L1-deficient gad mouse. *Brain Res.* **1019**, 1–9.

Wilkinson K. D. (1995) Roles of ubiquitinylation in proteolysis and cellular regulation. *Annu. Rev. Nutr.* **15**, 161–189.

Wilkinson K. D., Deshpande S. and Larsen C. N. (1992) Comparisons of neuronal (PGP 9.5) and non-neuronal ubiquitin C-terminal hydrolases. *Biochem. Soc. Trans.* **20**, 631–637.

Wilkinson K. D., Lee K. M., Deshpande S., Duerksen-Hughes P., Boss J. M. and Pohl J. (1989) The neuron-specific protein PGP 9.5 is a ubiquitin carboxyl-terminal hydrolase. *Science* **246**, 670–673.

Wong M. H., Saam J. R., Stappenbeck T. S., Rexer C. H. and Gordon J. I. (2000) Genetic mosaic analysis based on Cre recombinase and navigated laser capture microdissection. *Proc. Natl. Acad. Sci. USA* **97**, 12 601–12 606.

Xu G. Y. and Huang L. Y. (2004) Ca^{2+}/calmodulin-dependent protein kinase II potentiates ATP responses by promoting trafficking of P2X receptors. *Proc. Natl Acad. Sci. USA* **101**, 11 868–11 873.

Zhu Y., Carroll M., Papa F., Hochstrazin M. E. and D'Andrea A. D. (1996) DUB-1, a deubiquitinating enzyme with growth-suppressing activity. *Proc. Natl. Acad. Sci. USA* **93**, 3275–3279.

doi:10.1093/brain/awh368 *Brain* (2005), **128**, 405–416

The slow Wallerian degeneration gene, *Wld*^{S}, inhibits axonal spheroid pathology in gracile axonal dystrophy mice

Weiqian Mi,[1,*] Bogdan Beirowski,[1,2,*] Thomas H. Gillingwater,[3] Robert Adalbert,[1,4] Diana Wagner,[1] Daniela Grumme,[1] Hitoshi Osaka,[5,6] Laura Conforti,[4] Stefan Arnhold,[2] Klaus Addicks,[2] Keiji Wada,[5] Richard R. Ribchester[3] and Michael P. Coleman[1,4]

[1]*ZMMK and Institute for Genetics and* [2]*Department of Anatomy I, University of Cologne, Cologne, Germany,* [3]*Division of Neuroscience, University of Edinburgh, Edinburgh,* [4]*The Babraham Institute, Babraham, Cambridge, UK,* [5]*Department of Degenerative Neurological Diseases, National Institute of Neuroscience, Kodaira, Tokyo and* [6]*Clinical Research Institute, Kanagawa Children's Medical Center, Yokohama, Japan*

Correspondence: Dr Michael Coleman, The Babraham Institute, Babraham, Cambridge CB2 4AT, UK
E-mail: michael.coleman@bbsrc.ac.uk
**W. Mi and B. Beirowski contributed equally to this work*

Summary

Axonal dystrophy is the hallmark of axon pathology in many neurodegenerative disorders of the CNS, including Alzheimer's disease, Parkinson's disease and stroke. Axons can also form larger swellings, or spheroids, as in multiple sclerosis and traumatic brain injury. Some spheroids are terminal endbulbs of axon stumps, but swellings may also occur on unbroken axons and their role in axon loss remains uncertain. Similarly, it is not known whether spheroids and axonal dystrophy in so many different CNS disorders arise by a common mechanism. These surprising gaps in current knowledge result largely from the lack of experimental methods to manipulate axon pathology. The slow Wallerian degeneration gene, *Wld*^{S}, delays Wallerian degeneration after injury, and also delays 'dying-back' in peripheral nervous system disorders, revealing a mechanistic link between two forms of axon degeneration traditionally considered distinct. We now report that *Wld*^{S} also inhibits axonal spheroid pathology in gracile axonal dystrophy (*gad*) mice. Both gracile nucleus ($P < 0.001$) and cervical gracile fascicle ($P = 0.001$) contained significantly fewer spheroids in *gad/Wld*^{S} mice, and secondary signs of axon pathology such as myelin loss were also reduced. Motor nerve terminals at neuromuscular junctions continued to degenerate in *gad/Wld*^{S} mice, consistent with previous observations that *Wld*^{S} has a weaker effect on synapses than on axons, and probably contributing to the fact that *Wld*^{S} did not alleviate *gad* symptoms. *Wld*^{S} acts downstream of the initial pathogenic events to block *gad* pathology, suggesting that its effect on axonal swelling need not be specific to this disease. We conclude that axon degeneration mechanisms are more closely related than previously thought and that a link exists in *gad* between spheroid pathology and Wallerian degeneration that could hold for other disorders.

Keywords: axon; axonal spheroid; gracile axonal dystrophy; ubiquitin; Wallerian degeneration

Abbreviations: APP = amyloid precursor protein; *gad* = gracile axonal dystrophy; GFAP = glial fibrillary acidic protein; H & E = haematoxylin and eosin; NMJ = neuromuscular junction; PFA = paraformaldehyde; PNS = peripheral nervous system; *Wld*^{S} = slow Wallerian degeneration gene, mutation or mice; Wld^S = slow Wallerian degeneration protein; YFP = yellow fluorescent protein

Received April 17, 2004. Revised August 12, 2004. Accepted November 1, 2004. Advance Access publication January 11, 2005

Introduction

Axonal dystrophy and spheroids are hallmarks of CNS axon pathology. Axonal spheroids are focal 10–50 μm diameter swellings, which are sometimes, but not always, terminal endbulbs, and are filled with disorganized neurofilaments,

tubules, organelles or multi-lamellar inclusions. Dystrophic axons are usually smaller swellings often associated with continuity of the axon. One or both of these aberrant axon morphologies is found in a wide range of CNS neurodegenerative disorders, including stroke (Dewar *et al.*, 1999), myelin disorders (Griffiths *et al.*, 1998), tauopathies (Lewis *et al.*, 2000; Probst *et al.*, 2000), amyotrophic lateral sclerosis (Tu *et al.*, 1996; Oosthuyse *et al.*, 2001; Howland *et al.*, 2002), traumatic brain injury (Cheng and Povlishock, 1988), Alzheimer's disease (Brendza *et al.*, 2003), Parkinson's disease (Galvin *et al.*, 1999), Creutzfeldt–Jakob disease (Liberski and Budka, 1999), HIV dementia (Raja *et al.*, 1997; Adle-Biassette *et al.*, 1999), hereditary spastic paraplegia (Ferreirinha *et al.*, 2004) and Niemann–Pick disease (Bu *et al.*, 2002). They also occur during normal ageing and secondarily in some serious illnesses (Sung *et al.*, 1981). In contrast, peripheral nervous system (PNS) axons undergo 'Wallerian-like' or 'dying-back' degeneration, even in diseases where CNS axons form swellings (Miura *et al.*, 1993; Lewis *et al.*, 2000; Oosthuyse *et al.*, 2001), although swellings do also occur in some rare PNS disorders (Miike *et al.*, 1986; Bomont *et al.*, 2000).

The roles of axonal swellings in disease are poorly understood, as illustrated by the following examples. First, in multiple sclerosis, many large spheroids are terminal endbulbs of transected axons but there are also a few 'en passant' swellings of similar shape and dimension (Trapp *et al.*, 1998) and many small dystrophic swellings (Ferguson *et al.*, 1997; Kornek *et al.*, 2000, 2001). It remains unclear whether these different types of swelling have common or different origins. Secondly, it is not clear whether disease-specific mechanisms lead to a common final pathway of axonal dystrophy, as in Alzheimer's disease, stroke and multiple sclerosis, and if so how they do this. Thirdly, it is not known why swellings predominate in distal axons in some diseases, such as gracile axonal dystrophy (*gad*) (Yamazaki *et al.*, 1988; Mukoyama *et al.*, 1989), caused by loss of ubiquitin C-terminal hydrolase 11 (*Uch-l1*) (Saigoh *et al.*, 1999), while in other diseases they occur in proximal axons, as in amyotrophic lateral sclerosis (Tu *et al.*, 1996) and tauopathy (Probst *et al.*, 2000). Finally, a better understanding is needed of the relationship between axon swelling and impaired axonal transport. Amyloid precursor protein (APP) accumulates in axonal swellings and spheroids in stroke (Dewar *et al.*, 1999), traumatic brain injury (Gentleman *et al.*, 1993), multiple sclerosis (Ferguson *et al.*, 1997), Creutzfeld–Jakob disease (Liberski and Budka, 1999), HIV dementia (Raja *et al.*, 1997; Adle-Biassette *et al.*, 1999) and *gad* (Ichihara *et al.*, 1995), indicating that axonal transport is impaired. However, it is not known whether axon swelling in these disorders is simply a consequence of impaired axonal transport, or whether it causes the transport defect, or both. These and other important questions remain unanswered largely because experimental methods to manipulate axonal swelling have not been available.

A mutant mouse gene, Wld^S, blocks a rate-limiting step common to Wallerian degeneration and diverse PNS axon disorders, including dysmyelination (Samsam *et al.*, 2003), motor neuronopathy (Ferri *et al.*, 2003) and Taxol toxicity (Wang *et al.*, 2002). Recently, Wld^S was reported to be effective in acute CNS lesions modelling stroke (Gillingwater *et al.*, 2004) and Parkinson's disease (Sajadi *et al.*, 2004) but its effect in a chronic CNS disease has not been reported. Wld^S is a chimeric gene (Conforti *et al.*, 2000) formed by a stable triplication (Coleman *et al.*, 1998; Mi *et al.*, 2003) encoding the N-terminus of multiubiquitylation factor Ube4b fused in-frame to nicotinamide mononucleotide adenylyltransferase (Nmnat1) plus a short novel sequence (Mack *et al.*, 2001). Nmnat1 appears to be sufficient to confer the phenotype *in vitro*, but it is not yet clear whether this holds *in vivo* (Coleman and Perry, 2002; Araki *et al.*, 2004). Wld^S protein appears to be restricted to the nucleus, so its effect on axons is mediated by other factors (Mack *et al.*, 2001), which may include the NAD-dependent deacetylase SIRT-1 (Araki *et al.*, 2004).

To study the relationship between axonal swelling and Wallerian degeneration, we crossed Wld^S and *gad* mice. Wld^S significantly reduced spheroid numbers without altering the first stages of *gad* pathogenesis, revealing a link between Wallerian degeneration and axonal spheroids in this disease that could extend to other disorders.

Methods

Origin, breeding and genotyping of mice

Homozygous C57BL/Wld^S spontaneous mutants were obtained from Harlan UK (Bicester, UK) and mated with heterozygous *gad* mice, kindly provided by Professor Keiji Wada and Dr Hitoshi Osaka (National Institute of Neuroscience, Tokyo, Japan), following a cross to C57BL/6 to ensure a more homogeneous genetic background. Thus, the genetic background of the experimental mice was 75% C57BL/6, 12.5% CBA/Nga, 12.5% RFM/Nga. Double heterozygotes were identified in the F1 generation by genotyping for *gad* (below) and intercrossed. *gad* homozygotes were identified by genotyping and selected for further study. Wld^S genotype was determined *post mortem* by pulsed-field gel electrophoresis of spleen DNA (Mi *et al.*, 2002). Hemizygous yellow fluorescent protein (YFP) mice of line YFP-H were obtained from Jackson Laboratories (Bar Harbor, MN, USA) and mated with *gad*/Wld^S double heterozygotes. Triple heterozygotes were then mated to *gad*/Wld^S double heterozygotes to produce *gad* homozygotes that were heterozygous for both Wld^S and YFP-H. For *gad* genotyping, tail genomic DNA was extracted at 3 weeks using the Nucleon II kit (Amersham Pharmacia), digested with *Pvu*II, and Southern blotted. It was then hybridized with a ^{32}P-labelled 764-bp probe generated by PCR from *gad* homozygous genomic DNA using primers 5′-ATCCAGGCGGCCCATGACTC-3′ and 5′-AGCTGCTTTGCAGAGAGCCA-3′. Positively hybridizing fragments indicative of the *gad* (0.75 kb) and wild-type (1.6 kb) alleles were then identified by autoradiography. To genotype for inheritance of the YFP-H transgene, the skin of a 1–2 mm ear punch at 21 days was pulled apart and fluorescent axons identified using a Zeiss Axiovert S100 inverted fluorescent microscope through the FITC filter.

Assessment of Wallerian degeneration

gad homozygotes that were heterozygous for *Wld*^{S} and hemizygous for the *YFP-H* transgene were anaesthetized prior to the onset of hindlimb weakness using intraperitoneal Ketanest (100 mg/kg; Parke Davis/Pfizer, Karlsruhe, Germany) and Rompun (5 mg/kg; Bayer, Leverkusen, Germany). The right sciatic nerve (upper thigh) was transected and the wound closed with a single suture. Five days later the mice were killed by cervical dislocation, the swollen first 2 mm of distal sciatic nerve was discarded and the next 2 mm was used for western blotting for heavy neurofilament protein as previously described (Mack *et al.*, 2001). The tibial nerve of the operated leg with a minimum of attached non-nervous tissue was processed for YFP fluorescence as follows. The nerve was stretched by ~10% by pinning onto a Sylgard (Du Pont) dish and fixed with 4% paraformaldehyde (PFA) (BDH Laboratory, UK) in 0.1 M phosphate-buffered saline (PBS) in the dark for 1 h. It was then incubated in 1% Triton X-100 (Sigma, Germany) in 0.1 M PBS for 10 min and washed three times with PBS before mounting in Vectashield (Vector Laboratories, USA). The degree of fragmentation of the representative subset of motor and sensory axons that are YFP-labelled was determined. For more detail, see Beirowski *et al.* (2004).

Preparation of gracile tract sections

Mice aged 126–130 days were anaesthetized using Ketanest and Rompun (100 mg/kg and 5 mg/kg intraperitoneally, respectively) or a higher dose as required for deep terminal anaesthesia. After sternotomy mice were killed by cardiac puncture and instantly intracardially perfused first with a solution containing 10 000 IE/l heparin (Liquemin N 25000; Hoffmann-La Roche) and 1% procainhydrochloride in 0.1 M PBS for 30 s and then with fixative (4% paraformaldehyde in 0.1 M PBS) for 10 min. Brain and spinal cord were carefully removed, further fixed in 4% PFA/0.1 M PBS overnight and extensively washed in 0.1 M PBS. Fixed tissues were extensively rinsed in fresh 0.1 M PBS, dehydrated in an ascending ethanol series and subsequently embedded in paraffin (Paraplast; Sherwood Medical Co., St Louis, MO, USA) applying standard histology techniques. Coronal serial sections (6 μm) were made using a Type HM355 microtome (Microm GmbH) from the entire gracile nucleus in medulla oblongata and cervical gracile fascicle starting at level 535 (Sidman *et al.*, 1971). Serial paraffin sections were mounted on conventional glass slides for use in haematoxylin and eosin (H & E) staining or on poly-L-lysine-coated slides for use in Luxol Fast Blue staining and immunocytochemistry, alternating normally every 2–3 sections. Distinction between gracile nucleus and cervical gracile fascicle was made by applying histomorphological criteria for the typical shapes of coronal sections.

H & E staining and spheroid quantification

Six-micrometre sections were deparaffinized in xylol (Carl-Roth, Germany) for 10 min, rehydrated in a descending ethanol series and rinsed in deionized H_2O for 1 min. Sections were placed in haematoxylin for 5 min, rinsed in tap water for 1 min to allow stain to develop and then placed in eosin for 2 min, dehydrated and mounted in Entellan resin (Merck, Germany). The occurrence of clearly detectable eosinophilic spheroids, indicative of dystrophic axons (Yamazaki *et al.*, 1988; Mukoyama *et al.*, 1989; Kikuchi *et al.*, 1990) was quantified in ~90 sections uniformly dispersed throughout the gracile nucleus of each individual and ~30 sections uniformly dispersed throughout the cervical gracile fascicle. Analysis of lateral columns was performed on these same 30 sections, counting the sum of spheroid numbers on both sides of the spinal cord. In this way, irregular results due to local deviations in spheroid numbers could be ruled out. H & E stained axonal spheroids were generally eosinophilic and appeared glassy or hyaline with a round or oval shape. They varied in diameter (5–50 μm) and sometimes reached a size larger than the nerve cells in gracile nucleus. All specimens were scored blind and agreed by two independent investigators.

Luxol Fast Blue staining and densitometric quantification

Six-micrometre sections from equivalent points in *gad* and *gad/Wld*^{S} cervical spinal cord and medulla oblongata were processed simultaneously as follows. Sections were deparaffinized in xylol (Carl-Roth, Germany) for 15 min, and processed twice through 100% ethanol for 2 min and 96% ethanol for a few seconds. Slides were transferred to Luxol Fast Blue solution [0.1% Luxol Fast Blue MBS chroma (Merck), 10% acetic acid all made up in 96% ethanol] and incubated at 60°C for 5 h. Sections were then rinsed in 95% ethanol and distilled water for 1 min each, dipped in 0.05% lithium carbonate (Merck) for 1 min, and differentiated in 70% ethanol for a further 1 min. After rinsing in distilled water, sections were examined under light microscope for suitable differentiation between white and grey matter. Nuclear Fast Red staining was carried out for 10 min in 5% aluminium sulphate, 0.1% Nuclear Fast Red followed by rinsing in distilled H_2O, 90% ethanol and 100% ethanol for 1 min each. Slides were incubated in xylol for 5 min and mounted in Entellan resin (Merck). Slides were examined under light microscopy (Nikon Eclipse E200) and evaluated using Bioscan OPTIMAS 6.0 software (Optimas Corp., WA, USA) according to the manufacturer's instructions. For densitometric quantitation, mean grey values were obtained for circumscribed areas of interest using a three-chip monochrome CCD camera, and the background grey value (tissue-free area) was subtracted. Since demyelination occurs selectively in the gracile tract and not in the cuneate tract of *gad* mice by 126–130 days (Mukoyama *et al.*, 1989; our observations), we used cuneate fascicle as a reference area and expressed Luxol Fast Blue staining in gracile tract as a percentage of that in cuneate tract. We applied this procedure to representative Luxol Fast Blue-stained sections of cranial gracile tract: two sections from level C2/C3 representing the cervical gracile fascicle and two sections from level 535 representing the gracile nucleus (Sidman *et al.*, 1971).

Immunocytochemistry of gracile tract

Six-micrometre paraffin sections from equivalent points in *gad* and *gad/Wld*^{S} cervical spinal cord and medulla oblongata were processed simultaneously as follows. Sections were deparaffinized, rehydrated in a descending ethanol series, washed several times in 0.05 M Tris-buffered saline (TBS), and treated with a solution of 6% H_2O_2 in methanol for 20 min to block endogenous peroxidase activity. They were then permeabilized with 0.1% Triton X-100 (Sigma) in 0.05 M TBS additionally containing 0.05 M NH_4Cl, rinsed in fresh TBS three times and subsequently immunoblocked with 5% bovine serum albumin (Sigma) in 0.05 M TBS